



Calcite raft geochemistry as a hydrological proxy for Holocene aquifer conditions in Hoyo Negro and Ich Balam (Sac Actun Cave System), Quintana Roo, Mexico



Shawn E. Kovacs^{a,*}, Eduard G. Reinhardt^a, James C. Chatters^b, Dominique Rissolo^c, Henry P. Schwarcz^a, Shawn V. Collins^d, Sang-Tae Kim^a, Alberto Nava Blank^e, Pilar Luna Erreguerena^f

^a School of Geography and Earth Sciences, McMaster University, Hamilton, Ontario, L8S 4K1, Canada

^b Applied Paleoscience, 10322 NE 190th Street, Bothell, WA 98011, USA

^c Centre of Interdisciplinary Science for Art, Architecture, and Archaeology (CISA3), University of California, San Diego, CA 92093-0436, USA

^d Clarion University, Department of Biology and Geosciences, Clarion, PA, 16214, USA

^e Bay Area Underwater Explorers, CISA3/UCSD, Berkeley, CA, USA

^f Subdirectora de Arqueología Subacuática, Instituto Nacional de Antropología e Historia, Calle Moneda No. 16, Col. Centro Histórico México, D.F. 06060, Mexico

ARTICLE INFO

Article history:

Received 27 April 2017

Received in revised form

11 September 2017

Accepted 14 September 2017

Available online xxx

Keywords:

Calcite rafts

Coastal karst aquifers

Yucatán

Climate

Sea-level

Aquifer salinity

Potable water

Calcite raft cones

Paleoamericans

ABSTRACT

Two cores from calcite rafts deposits located in Cenote Ich Balam and Hoyo Negro were dated and analyzed for $^{87}\text{Sr}/^{86}\text{Sr}$, $\delta^{18}\text{O}$, $\delta^{13}\text{C}$, Sr/Ca and Cl/Ca. The geochemical records show changing aquifer salinity spanning the last ~ 8.5 cal kyrs BP and interrelationships with Holocene climate trends (wet and dry periods). During the wet mid-Holocene, the salinity of the meteoric Water Mass (WM; at 7.8–8.3 cal kyrs BP) was relatively high at 1.5–2.7 ppt and then became less saline (1.0–1.5 ppt) during the last ~ 7000 yrs as climate became progressively drier. High salinity of the meteoric WM during the wet mid-Holocene is attributed to increased turbulent mixing between the meteoric and underlying marine WM. Increased precipitation, in terms of amount, frequency, and intensity (e.g. hurricanes) causes higher flow of meteoric water towards the coast and mixing at the halocline, a phenomenon recorded with recent instrumental monitoring of the aquifer. Conversely, during dry periods reduced precipitation and flow in the meteoric WM would result in lower salinity. Karst properties and Holocene sea-level rise also seem to have an effect on the aquifer. When the regionally extensive network of shallow cave passages (~ 10–12 m water depth) are flooded at ~ 8000 cal yrs BP, there is a rapid shift in salinity. This study demonstrates that calcite raft deposits can be used as paleo-environmental recorders documenting the effects of sea level and climate change on aquifer condition.

© 2017 Elsevier Ltd. All rights reserved.

1. Introduction

Human skeletal fossils from phreatic coastal karst systems on the eastern margin of the Yucatán Peninsula show early Pre-Ceramic migration and settlement in the Yucatán at the end of the Pleistocene (González et al., 2008, 2013, 2016). Recently, a well-preserved, age-constrained Late Pleistocene (13–12 cal kyrs BP) female skeleton [*Homo sapiens*] was found in the Hoyo Negro (HN) pit cave (Naia; HN-5/48; Chatters et al., 2014). Her cranial and

dental features share morphometric similarities with other early Paleoamericans, but she has (mt)DNA of Native Americans (Chatters et al., 2014, 2017). HN represents the first and only example of a human skeleton found in direct association with now-extinct Pleistocene megafauna in the Americas (Chatters et al., 2014; Collins et al., 2015). The study of the fossil record in HN is still ongoing, but there are many questions on how early Paleoamerican migrants adapted and subsisted on the Yucatán landscape. The prevailing view is that Naia and the animals entering the cave were in search of water, although there is no geological information on the condition of the aquifer during the Pleistocene/Holocene to substantiate this claim.

* Corresponding author.

E-mail address: kovacs2@mcmaster.ca (S.E. Kovacs).

Calcite raft deposits which have extensive distributions throughout Yucatán caves could possibly provide insights into how the potability (i.e. salinity) of the aquifer has changed with Holocene climate and sea-level. Calcite rafts have many advantages as they form abiotically at the air/water interface documenting the upper aquifer, preserve well in the stratigraphic record, and they accumulate on the bottom in large stratified piles. However, despite these advantages, they have never been used before in paleo-environmental studies.

1.1. Hydrological setting

The Yucatán Peninsula is the aerially emergent portion of the greater Yucatán Platform, a vast limestone platform with a surface area of 300 000 km² (Bauer-Gottwein et al., 2011). The Peninsula itself encompasses over 165 000 km² of the total surface area, separating the Caribbean Sea from the Gulf of Mexico, and consists of Cenozoic Era biogenic limestone (Fig. 1; Ward et al., 1985).

The climate is tropical with distinct wet and dry seasons (Kottke et al., 2006). Monthly average temperatures range between 23 and 29 °C, with an average annual temperature of 26 °C. The hot/wet season is from May to November, whereas the relatively cooler dry season is from December to April (Hodell et al., 2007). Seasonal precipitation is determined by the movement of the ITCZ, which is controlled by the strength and movement of the Bermuda High and the easterly trade winds (Fig. 1; Hastenrath, 2012). Neuman and Rahbek (2007) document a significant east-west precipitation gradient across the Peninsula, with most of the precipitation (80%) falling on the Caribbean coast (>1500 mm/yr) during the summer wet season (González-Herrera et al., 2002). Quintana Roo surface soil coverage is sparse and thin, hosting a tropical arid forest comprised of palms (i.e. rain trees), broad-leafed trees and succulents (Bautista et al., 2011).

The landscape has low-lying topography that has been extensively karstified by the interaction of glacioeustasy, littoral processes and mixing-zone hydrology (Smart et al., 2006). Consequently, precipitation rapidly infiltrates through the limestone to a shallow, density stratified, unconfined coastal aquifer

(Perry et al., 2003; Beddows et al., 2007). Hydrogeology of the aquifer is influenced by the porous nature of the limestone, which features structural heterogeneities (fissures and fractures), high matrix porosity, and karstic conduits (Kambesis and Coke, 2013). There is little surface drainage with no rivers and only a few lakes (Perry et al., 2003).

In anchialine settings, which characterize many karst coastlines, a meteoric Water Mass (WM) rests on a marine WM intruding from the coast that is separated by a halocline transition zone. In HN, the meteoric WM has a salinity of 1.1 ppt vs 35.1 ppt in the marine WM, and the current position of the halocline is at –18.5 m (all depths are relative to local water level unless otherwise stated; Fig. 3). The salinity of the meteoric WM varies spatially with areas closer to the coast having higher salinity than inland areas (Kovacs et al., 2017a). The interaction between the meteoric and marine WM is poorly understood in space and time, with few available paleo-environmental records to understand how meteoric WM salinity may have been affected by climate and sea-level change (Kovacs et al., 2017a). Consequently, we do not know whether the groundwater was potable at the end of the Pleistocene or the early Holocene, when the climate was dry and when early Paleoamericans arrived to the Yucatán (Chatters et al., 2014; Haug et al., 2001). Groundwater may have been quite important to early migrants who did not construct cisterns to store rainwater (i.e. Maya) and there were few lakes to rely upon for freshwater (Metcalf et al., 2000). Therefore, groundwater from caves and cenotes may have provided a year-round water supply for early Paleoamericans, but with low sea level and thus groundwater during the early Holocene, only deep caves and pits would have provided access. The spatial extent of these deep access points may have influenced settlement and restricted movement on the landscape for early Paleoamericans.

1.2. Hoyo Negro and Ich Balam

HN is located on eastern coast of the Yucatán Peninsula (Quintana Roo) within the Outland Cave System, which is a distributary branch of the larger Sac Actun Cave system that has > 257 km of mapped passage (Figs. 1 and 2; Quintana Roo Speleological Survey,

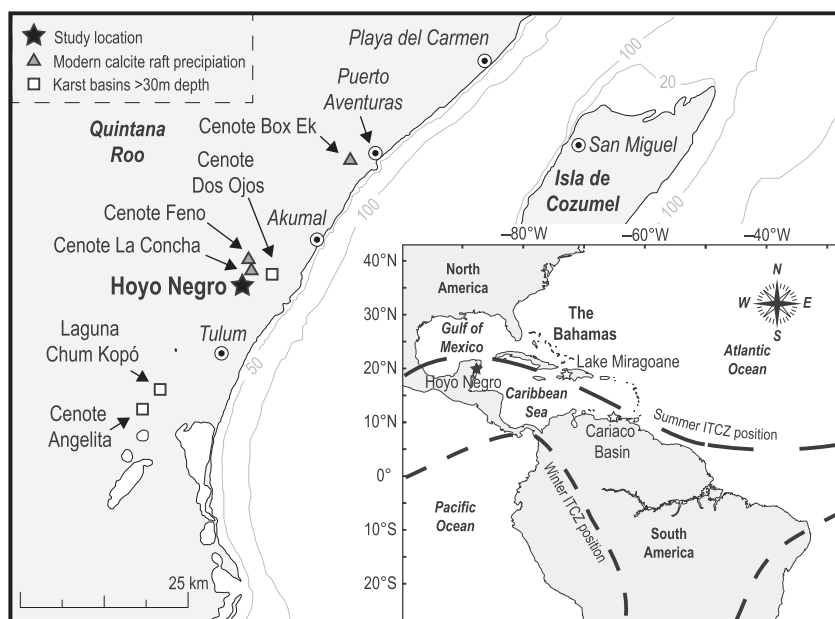


Fig. 1. Map showing the geographical position of HN and other cenotes used in this study. Bathymetric contours are represented in meters. Inset shows location of Cariaco Basin (Venezuela) and the summer/winter position of the Atlantic Intertropical Convergence Zone (ITCZ).

2017). HN is a bell-shaped dissolution chamber which is ~ 37 m in diameter at the top (-12 m) and ~ 62 m in diameter at the bottom (-48 m). The pit floor consists of large fragments of limestone breakdown from the overlying ceiling with patchy accumulations of bat guano, seeds, calcite raft-piles, twigs, branches, and charcoal (Chatters et al., 2014; Collins et al., 2015).

HN is connected to Cenote Ich Balam (IB) but also more distal cenotes (e.g. Oasis; Fig. 2) via shallow cave passages. IB has a small opening of ~ 3.5 m² in the cavern ceiling and the drop to the present water surface is ~ 10 m. The center of the cavern contains a large breakdown pile of limestone with the top of the pile at -2.5 m which gradually slopes to -11 m at the periphery. The breakdown pile is covered with seeds, twigs, fine organic matter (OM) and calcite rafts.

Due to high porosity and permeability of the karst terrain, groundwater levels in IB, HN and the surrounding region closely track Holocene sea level (Collins et al., 2015; Gabriel et al., 2009; Smart et al., 2006). Groundwater level rises inland relative to sea level (~ 10–15 cm/km; Beddows, 2004; Beddows et al., 2007) and HN is ~ 7 km from the coast so local water level is ~ 1 m above msl (mean sea-level). As a result, when sea level was low, the region's maze of subterranean passageways would have been accessible to terrestrial animals and humans. Most of the cave passages in Quintana Roo today are relatively shallow at ~ 10 to 12 m water depth (Quintana Roo Speleological Survey, 2017), which is also the case for IB and HN. However, unlike other cave systems in the area, the cave passage in HN drops to - 48 m in a large circumference pit that contains skeletal remains of many extinct animals as well as *Naia*. HN is accessible from the surface via cave passages that connect with proximal and more distal cenotes (Fig. 2; e.g. Cenote IB and Cenote Oasis). Animals may have willingly entered the cave through accessible caverns in search of water and carrion, but may have also inadvertently fallen through the cave ceiling opening in IB as they wandered through the forest (a natural trap; Fig. 2; Chatters et al., 2014; Collins et al., 2015). Animals moving through the upper

cave passages would have fallen into HN as they navigated the lightless conditions. Humans may have entered the cave with torches in search of water or for ceremonial purposes (burial; González et al., 2008). In *Naia*'s case, speculation is she may have slipped and fallen into the pit while accessing groundwater, although it is unknown whether the groundwater was potable at that time.

1.3. Caribbean sea level and groundwater

Numerous studies have documented the de-glacial sea-level history of the Caribbean region (i.e. Blanchon et al., 2002; Blanchon and Shaw, 1995; Fairbanks, 1989; Lighty et al., 1982). Toscano and Macintyre (2003) created a western Atlantic sea-level curve that encompasses both coral and intertidal peat sea-level proxies. Their curve constrains the lower and upper boundaries of sea level, but does not account for glacio-isostatic adjustment of the crust (Blanchon, 2005; Toscano and Macintyre, 2003, 2006). However, far-field locations that are both tectonically stable, and experience a sea-level history independent of glacial isostatic adjustment (GIA), are a good approximation of eustasy (Milne and Mitrovica, 2008; Milne and Peros, 2013; Peltier and Fairbanks, 2006). The Yucatán has been tectonically stable since the Late Pleistocene (Ward et al., 1985), and therefore the glacio-eustatic sea-level history from the Circum-Caribbean region can be used to infer sea-level position on the Yucatán coast (Bard et al., 2010, 1996; Milne and Mitrovica, 2008; Milne and Peros, 2013). Based on the water level indicators from HN, the Medina-Elizalde (2013) GIA corrected sea-level curve fits better with the cave depositional record (Fig. 4; Collins et al., 2015). The timing for the flooding of the bottom of HN (>12–13 cal kyrs BP) has been constrained based on skeletal taphonomy; the animal skeletons including *Naia* are largely disarticulated and spatially scattered on the pit bottom, indicative of floating decomposition in a body of water (Chatters et al., 2014).

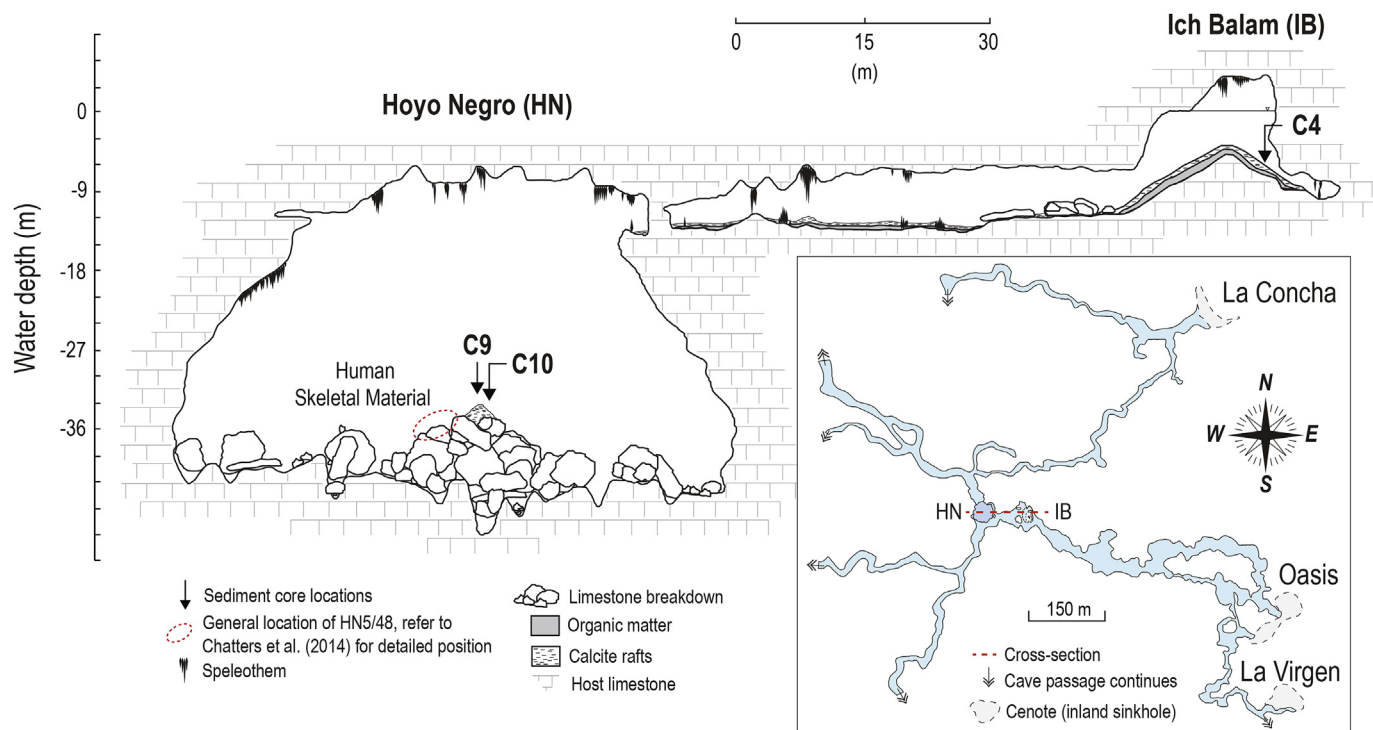


Fig. 2. Cross-section of the cave system showing core locations. Depths are relative to local water level which is -1–2 m above msl (see text for details). Inset shows a plan view of cave passages connecting to HN and cenotes in the immediate area.

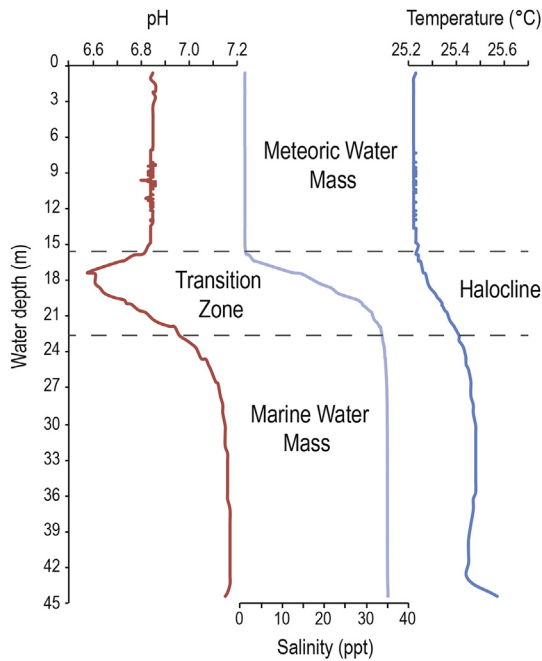


Fig. 3. HydroLab™ water mass profiles recorded in HN. The halocline transition zone is shown as a hatched line. Depths are relative to local water level.

1.4. Calcite rafts

Floating “rafts” of microcrystalline calcite (Fig. 5), commonly referred to as calcite rafts, are autochthonous CaCO_3 deposits that precipitate at the air-water interface in cave environments (Taylor and Chafetz, 2004). Calcite rafts form in CaCO_3 saturated waters through CO_2 degassing and/or evaporation (Gázquez and Calaforra, 2013; Hill and Forti, 1997; Jones, 1989; Taylor et al., 2004; Taylor

and Chafetz, 2004; van Hengstum et al., 2011). The polycrystalline aggregates eventually sink, as a result of surface tension of the raft being exceeded by gravitational forces and/or agitation of the surface water through hanging roots or drip water. The point source of water agitation and calcite raft sedimentation then forms conical shaped piles on the cave bottom. Smaller raft piles may coalesce with time, forming larger accumulations or may form sheet-like distributions on the cave bottom if there are larger surface water disturbances or currents transporting the calcite rafts (e.g. waves or currents in open caverns; Fornós et al., 2009; Gázquez and Calaforra, 2013; Taylor and Chafetz, 2004; van Hengstum et al., 2011). Calcite raft piles are also referred to as calcite raft cones or tower cones and may be unconsolidated or cemented together (Gázquez and Calaforra, 2013). We use the term “piles” vs. “cones” as piles infers sediment accumulating from above, and has stratigraphic connotation in terms of layers accumulating with relative age. “Pile” also fits better with other terms such as “mounds” and “sheet-like”, which we use to describe other calcite raft accumulations.

Collins et al. (2015) cored and documented the distribution and age of the calcite raft deposits in HN and IB, and used them to reconstruct cave flooding history. Kovacs et al. (2017b) documented seasonal trends in calcite raft precipitation using environmental monitoring and sediment traps in three nearby locations (Cenotes Rainbow, Feno and Monkey Dust) and showed rafts are precipitating throughout the year, with only minor hiatuses (i.e. days) during dilution of surface waters with large rainfall events. They also showed that calcite rafts were accumulating on the bottom using sediment traps at the monitoring locations. There are many advantages to using calcite rafts as a paleohydrological proxy. They: 1) form at the air-water interface providing records of the upper meteoric WM, 2) are a triphasic system (water-air-mineral) and thus are a useful indicator of past water levels within a cave system (i.e. presence of water; Collins et al., 2015), 3) form abiotically, implying no vital effects for the trace element and/or isotopic systems, and 4) are mineral material and thus readily preserve in

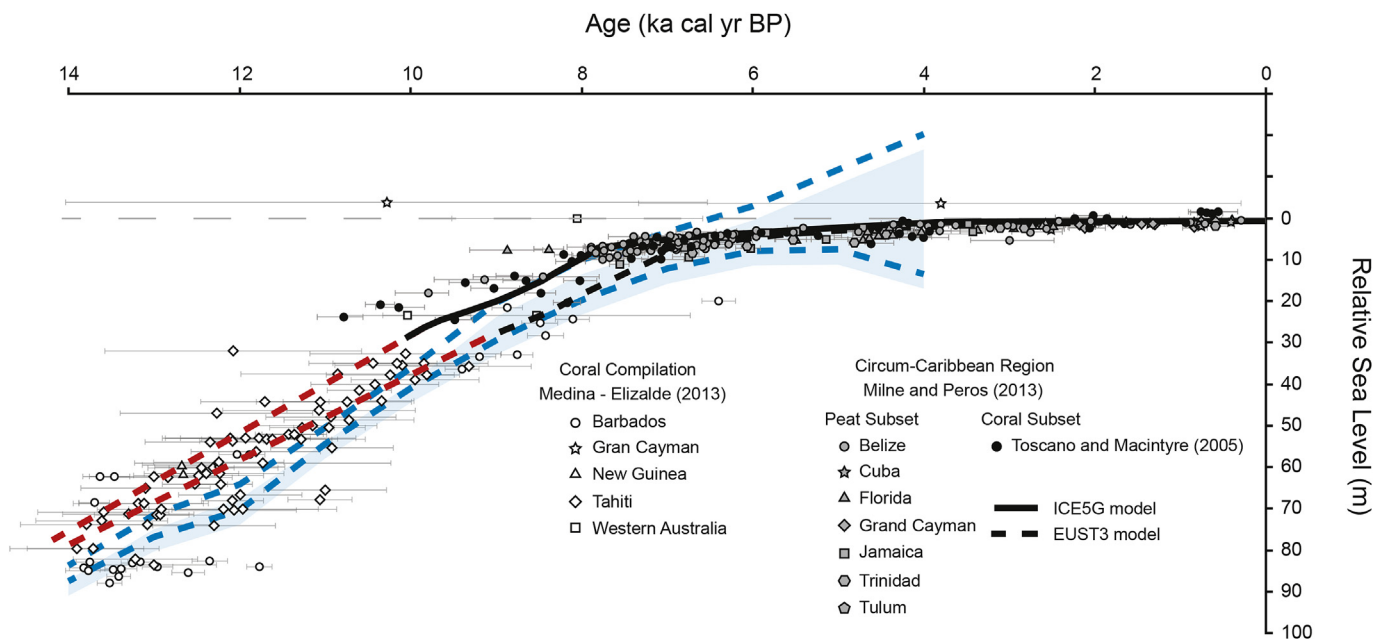


Fig. 4. Compilation of relative sea-level data used to infer flooding history of HN. Depths are in meters relative to mean sea level (msl). Data includes peat and coral records (Medina-Elizalde, 2013; Milne and Peros, 2013). The red dashed line represents a linear extrapolation for determining initial flooding (inundation) of the HN. The blue dashed line represents the global relative sea level model (Medina-Elizalde, 2013) while shaded area represents the glacial isostasy adjustment-corrected model for relative sea level rise (Bard et al., 2010). (For interpretation of the references to colour in this figure legend, the reader is referred to the web version of this article.)

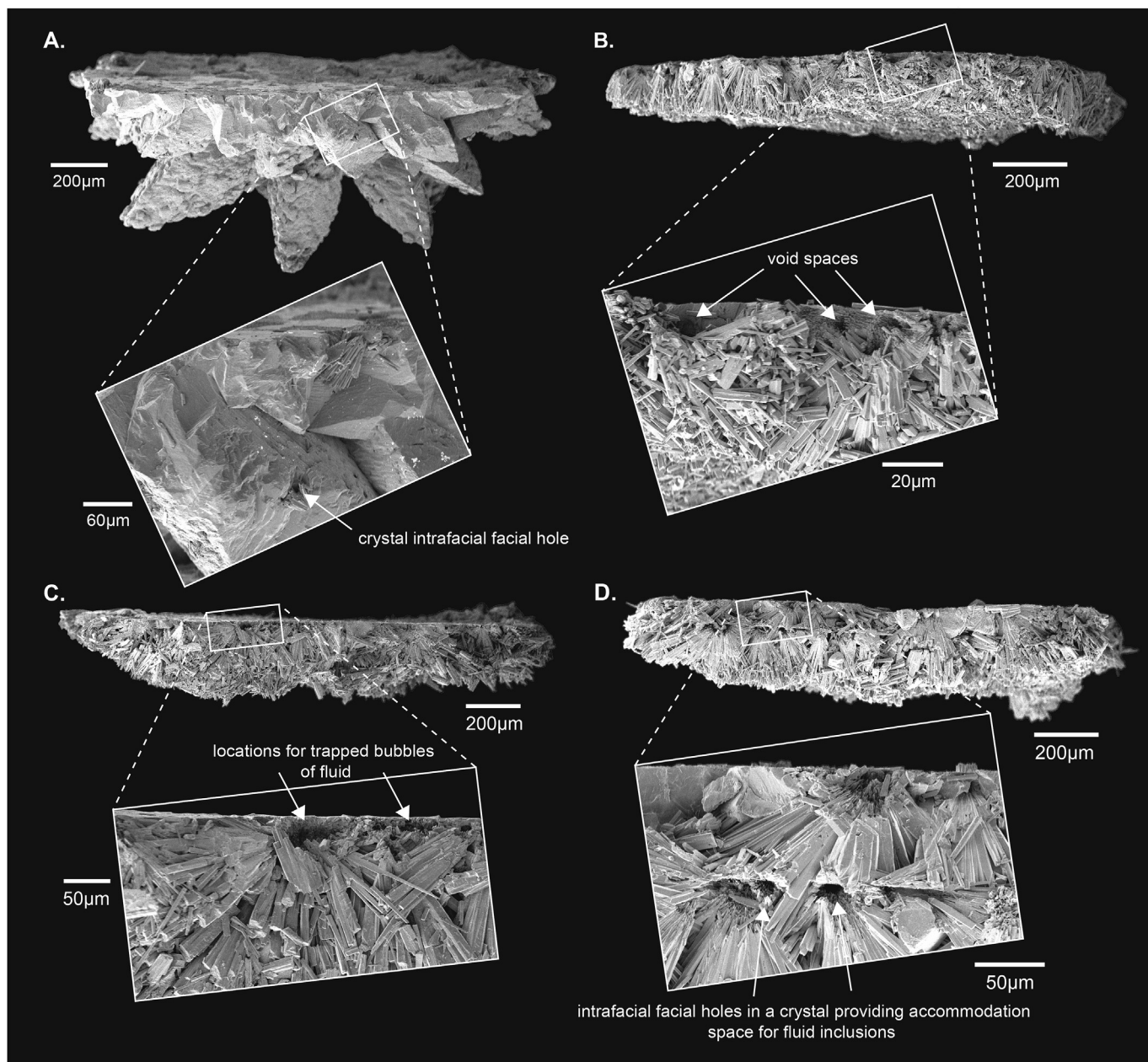


Fig. 5. Scanning electron microscope (SEM) images showing cross-sectional profiles through calcite rafts from varying depths in C9. Depths were selected at random A) 1–2 cm interval, B) 11–12 cm interval, C) 24–25 cm interval and D) 33–34 cm interval.

the stratigraphic record. Despite these advantages, there are no studies using calcite rafts to document past groundwater and climate conditions and this study from HN is the first to do so.

1.5. Geochemical proxies of salinity

Previous research used $^{87}\text{Sr}/^{86}\text{Sr}$ in biotic and abiotic carbonates as a paleosalinity proxy in marginal marine environments (Bryant et al., 1995; Holmden and Hudson, 2003; Peros et al., 2007; Reinhardt et al., 1998). Using a two-component mixing equation ($^{87}\text{Sr}/^{86}\text{Sr}$, [Sr]), deviations from the worldwide marine value ($^{87}\text{Sr}/^{86}\text{Sr} = 0.709175$) can be attributed to fresh-water dilution (McArthur et al., 2001). Salinity can be calculated if the fresh and marine water end-members are known or can be estimated (Reinhardt et al., 1998). A limitation of the method relates to the

concentration of Sr in marine waters (~ 8 ppm) which is much higher than in fresh (<1 ppm) water (Palmer and Edmond, 1992). Thus, a large dilution by fresh water is required to alter the $^{87}\text{Sr}/^{86}\text{Sr}$ ratio of marine waters, resulting in a hyperbolic mixing relationship. The method is best suited for determining lower salinities found in coastal systems (i.e. estuaries) but equally applicable to anchialine aquifers. Sr isotopes are also often paired with O and C isotopes, as well as trace elements since these analyses are relatively lower-cost providing higher resolution records (Sr/Ca; e.g. Holmden et al., 1997; Peros et al., 2007; Reinhardt et al., 2001). However, $\delta^{18}\text{O}$ and $\delta^{13}\text{C}$ values can be affected by processes other than mixing of fresh and marine water, including vital effects during biotic CaCO_3 precipitation, evaporation or changes in the isotopic composition of the fresh and marine water end-members (i.e. vegetation or precipitation; McDermott, 2004; Reinhardt

et al., 2001). Most research using O and C isotopes has been conducted on biotic CaCO₃ precipitates in marginal marine coastal environments, but can be applied to abiotic calcite rafts as well.

There has been little research on chlorine in carbonate sediments; most studies measured Cl⁻ extracted from pore fluid from sediment cores which is labor intensive and results in low stratigraphic resolution (e.g. Lazar et al., 2014; Levy et al., 2017). Chlorine however, can be measured using XRF core scanning which offers significant advantages in terms of resolution (<200 μm) and analytical efficiency but has not yet been extensively applied as a paleosalinity proxy. Recently, Peros et al. (2017) used Cl⁻ measured via XRF core scanning to document increased salinity and aridity in Cenote Jennifer, Cuba during the 8.2 yrs B.P event in the Caribbean and Chagué-Goff et al. (2016) found relationships between Cl⁻ and marine diatom assemblages showing past marine water incursions into a coastal lake in the Cook Islands.

2. Methodology

2.1. Cores

Multiple cores (n = 12; diam. 6 cm) were collected in IB and HN with locations and stratigraphy described in Collins et al. (2015). Cores were recovered using SCUBA and used a combination of pushing and percussion to penetrate the calcite raft pile. Core caps applied before extraction provided suction and retention of sediment in the core tube (see Collins et al., 2015 for details).

Calcite rafts and organic material (OM) cover the limestone breakdown pile in the center of IB, while the calcite raft piles in HN had a distinct cone geometry (~2.5 m in diameter and 1 m high) with several coalescing lobes (Fig. 6). Calcite raft piles are not abundant on the bottom of HN and the calcite raft distribution is mostly thin, low-profile coverings on the breakdown limestone. Two cores were selected for geochemical analysis, Core 4 (C4; ~65 cm) was from -12.3 m depth in IB and Core 9 (C9; ~45 cm) was collected in the largest calcite raft pile on the bottom HN at -42 m depth. These cores were sampled at 1 cm intervals by Collins et al. (2015). An additional core (Core 10; C10) was collected adjacent to Core 9 in HN (approx. 5 cm away) and in the same raft pile. There were no cemented laminae or indurated layers in the cores. Calcite raft imaging was performed using a JEOL 6610LV Scanning Electron Microscope (SEM) at the Canadian Centre for Electron Microscopy (CCEM; McMaster University).

2.2. Isotopic analysis

Oxygen and carbon isotope analyses on aliquots of ~100 μg CaCO₃ (n = 53) were conducted at McMaster University, Hamilton Ontario (Research Group for Stable Isotopologues - MSRI) using a VG Autocarb system attached to an Optima stable isotope ratio mass spectrometer. δ values are expressed in permil (‰) relative to Vienna PeeDee Belemnite (VPDB). The precision of the analyses is ±0.05‰ for both δ¹³C and δ¹⁸O and are calibrated with NBS 19 and NBS 18 calcite standards. Samples for strontium isotope analysis (n = 19) were dissolved in 1 M HCl, then separated using cation exchange columns and a Sr selective crown ether resin (Pin and Bassin, 1992). Analyses used a VG 354 multi-collector mass spectrometer in the Radiogenic Isotope Laboratory at McMaster University. National Bureau of Standards (NBS) 987 yielded a ⁸⁷Sr/⁸⁶Sr ratio of 0.71025 ± 2 × 10⁻⁵ on replicate analyses.

2.3. Elemental analysis

Elemental composition was measured using an ITRAX-XRF core scanner (Cox Analytical Systems; X-ray Fluorescence) at the

McMaster University Core Scanning Facility. Individual samples from C4 and C9 were rinsed with deionized water before analysis to remove any pore water and the intact C10 was flushed several times by adding deionized water at the top and allowing it to percolate and drain through the bottom. Previously sampled cores (C4 and C9) used a sequential sample holder to analyze the sediment at 1 cm intervals (Gregory et al., 2017). Each sample reservoir (~1 cm³) was evenly packed with sediment and analyzed using the Cr heavy element (Cr-HE) X-ray source (30kV, 10 mA, exp. time = 15 s, step-size = 200 μm). Ten measurements from the central portion of each sample reservoir were averaged. The intact C10 was analyzed with similar parameters as the sampled core (C9) for comparative purposes (Fig. 10).

2.4. Paleosalinity

Salinity can be estimated with a two-component mixing equation using the fresh and marine water end-member Sr concentrations ([Sr]; ppm) and ⁸⁷Sr/⁸⁶Sr values (e.g. Peros et al., 2007; Reinhardt et al., 2001). However, the mixing relationship can also be empirically derived using ⁸⁷Sr/⁸⁶Sr measurements from waters over a range of salinities. We calibrated our mixing curve using data from three cenotes that are precipitating calcite rafts: Box Ek, La Concha, and Feno, which are in a landward transect from the coast (located at 2.43 km, 6.46 km and 6.70 km). Salinities in the three locations were 2.6 ppt, 1.1 ppt and 1.3 ppt respectively, and had ⁸⁷Sr/⁸⁶Sr values (0.70845, 0.70825, 0.70834) that reflect salinity relative to mixing with modern seawater (0.709175 @ 35 ppt; Fig. 7). Hodell et al. (2004) recorded an ⁸⁷Sr/⁸⁶Sr value of 0.70831 for the surface waters of Aktun Ha and salinity was measured in 2007 at 1.5 ppt in van Hengstum et al. (2009; Fig. 7).

Conductivity and strontium concentrations of cenote water were measured by Actlabs Activation Laboratories Ltd. (Ancaster, Ontario, Canada). A Perkin Elmer Sciex ELAN 9000 Inductively Coupled Plasma Mass Spectrometry (ICP-MS) was used to determine strontium concentrations. Salinity was calculated using software from Five Creeks™ (<http://www.fivecreeks.org/monitor/sal.html>).

Water mass characteristics (temperature, pH and salinity) were measured using a calibrated MS5 Hydrolab MiniSonde® (June 4th, 2011). The sonde was gradually lowered through the water column in HN using SCUBA (Kovacs et al., 2017a).

2.5. Radiocarbon dating

Calcite rafts and seeds were ¹⁴C dated by DirectAMS™ in Seattle, Washington, U.S.A. Six paired seed/calcite rafts ¹⁴C ages were used to estimate the hard-water effect. Seeds and calcite rafts were selected from the same intervals in C4 and C9, but additional samples were also obtained from cores C3, C5, C6 described in Collins et al. (2015; Table 1). Seeds were pretreated using an acid/alkali/acid wash prior to analysis and calcite rafts were cleaned with deionized water. A hard-water offset of ~1300 ¹⁴C years BP was obtained for all samples (Fig. 8) and is similar to that found by Curtis et al. (1996; 1200–1300 yrs). The ¹⁴C activity of the dissolved inorganic carbon (DIC) in the water column in HN was also analyzed at the WM Keck Carbon Cycle AMS Laboratory at UC Irvine (Table 2). The DIC in the meteoric WM measured at -12 m had an age offset of ~1600 ¹⁴C years BP, which is consistent with our value (~1300 ¹⁴C years BP) from the calcite rafts which records the upper surface water DIC.

Dates are calibrated using the northern hemisphere terrestrial calibration curve IntCal13.14C (Reimer et al., 2013) using the R statistical software package Clam and a hard-water effect of 1300 yrs based on our estimate (Blaauw, 2010; version 2.2, Table 1).

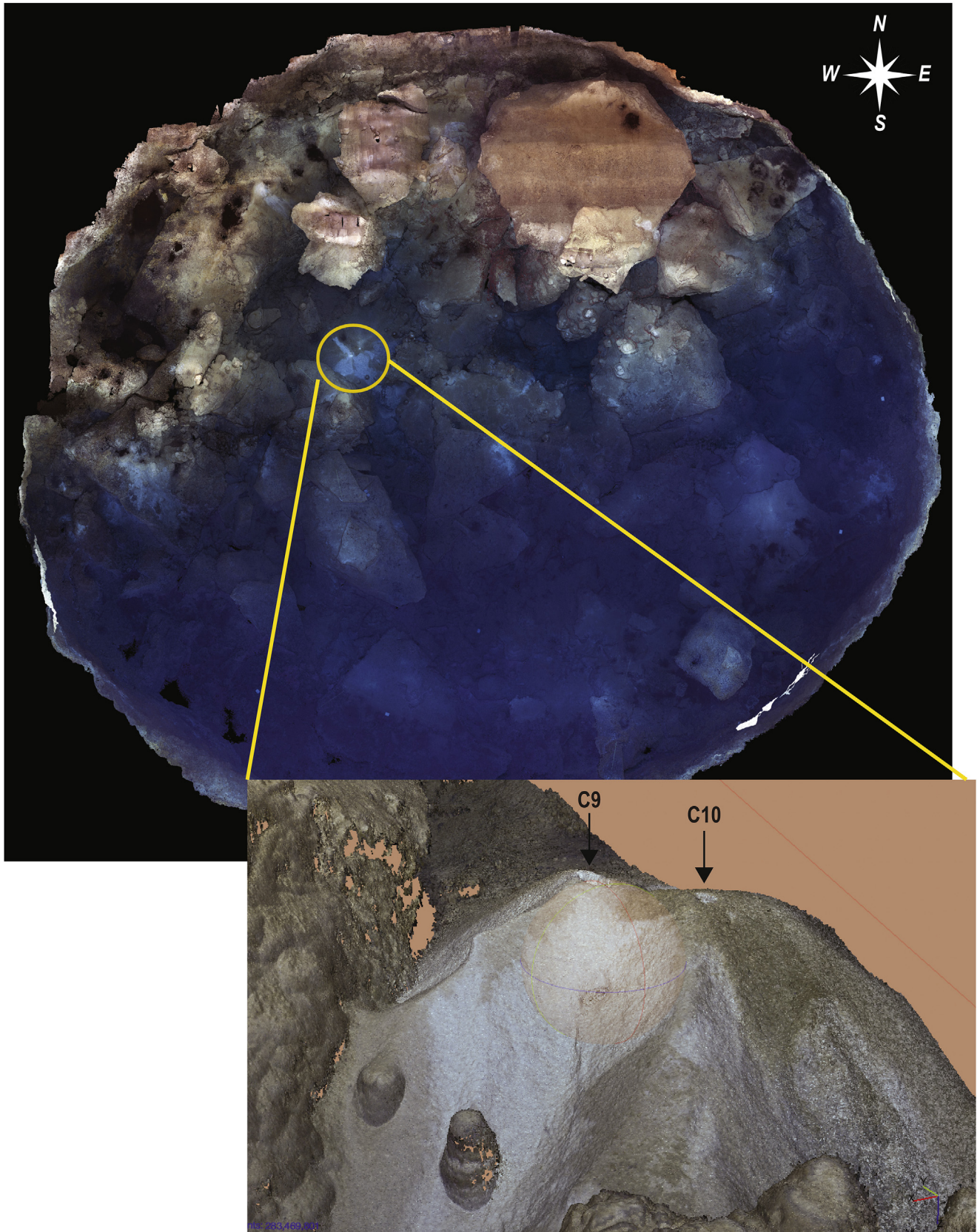


Fig. 6. Underwater photomosaic of HN compiled from 2200 images aligned on a 3-D model and projected in 2-D. Detailed 3-D image shows the geometry of the calcite raft pile and core locations (C9 and C10). Pit bottom is ~ 62 m in diameter.

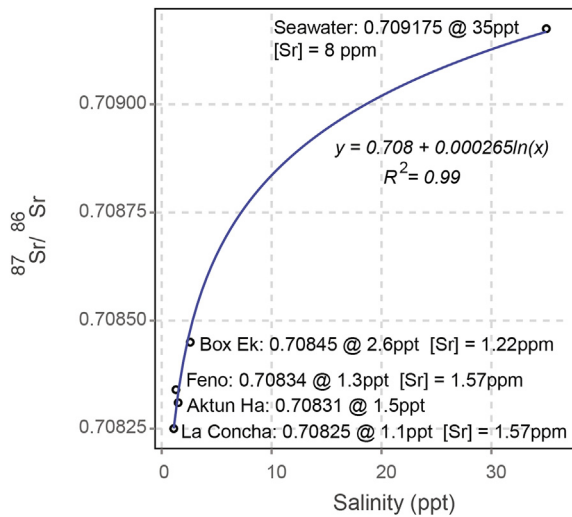


Fig. 7. Salinity mixing curve empirically compiled with salinity (ppt) and $^{87}\text{Sr}/^{86}\text{Sr}$ measured from calcite rafts precipitating in nearby cenotes.

Table 1
Radiocarbon results. * from Collins et al. (2015).

Lab ID	Core Interval	Material	$\delta^{13}\text{C}$ (‰)	^{14}C years BP	1σ
D-AMS 006412	IB-C3-7–8 cm	CR	–8.8	7332	32
D-AMS 002371	IB-C3-8 cm*	SD	–28.9	5990	32
D-AMS 006413	IB-C3-21–22 cm	CR	–10.7	7545	33
D-AMS 002369	IB-C3-22 cm*	SD	–33.5	6400	39
D-AMS 005586	IB-C4-1–2 cm	CR	–5.1	1848	26
D-AMS 005587	IB-C4-17–18 cm	CR	–5.7	4145	27
D-AMS 005588	IB-C4-33–34 cm	CR	–9.4	4744	29
D-AMS 005589	IB-C4-49–50 cm	CR	–8.1	5973	32
D-AMS 005590	IB-C4-63–64 cm	CR	–5.4	7328	32
D-AMS 005591	IB-C4-63–64 cm	SD	–38.9	6156	33
D-AMS 002373	IB-C5-107 cm*	SD	–26.9	5909	35
D-AMS 006414	IB-C5-106–107 cm	CR	–8.7	7017	33
D-AMS 002372	IB-C6-26 cm*	SD	–26.4	3510	31
D-AMS 006415	IB-C6-25–26 cm	CR	–6.9	5461	32
D-AMS 005592	HN-C9-0–1 cm	CR	–3.7	8258	36
D-AMS 005593	HN-C9-10–11 cm	CR	–4.2	8353	34
D-AMS 005594	HN-C9-21–22 cm	CR	–1.6	8459	35
D-AMS 005595	HN-C9-30–31 cm	CR	–3.5	8468	32
D-AMS 005596	HN-C9-43–44 cm	CR	–6.1	8747	33
D-AMS 005597	HN-C9-45–46 cm	CR	–6.3	9709	38
D-AMS 003404	HN-C9-46 cm*	SD	–33.8	8826	31

Five calcite raft samples (1–2, 17–18, 33–34, 49–50 and 63–64 cm) and one seed (63–64 cm) are used for C4, and six calcite raft samples (0–1, 10–11, 21–22, 30–31, 43–44, and 45–46 cm) and one seed (45–46 cm) for C9 (Table 1).

3. Results

3.1. Age models and accumulation rates

Core 9 in HN shows rapid accumulation (~ 45 cm) over approximately 400 yrs from 7900 to 8300 cal yrs BP (~ 0.11 cm/yr; Fig. 9). This accumulation rate is fairly high relative to the modern sediment trap studies in Kovacs et al. (2017b), but that rate (0.007 cm/yr) was from only three sites and represents only 2 years of measurement, so we do not have extensive data for comparison. In contrast, the accumulation rate for C4 from IB is lower. The accumulation rate over approximately 7000 cal yrs BP in C4 is ~ 0.010 cm/yr and is very similar to the accumulation rate that was calculated in Kovacs et al. (2017b).

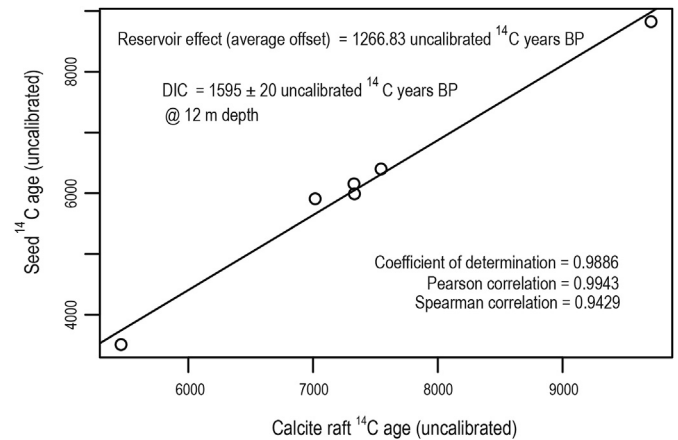


Fig. 8. Reservoir correction based on paired seed and calcite raft radiocarbon ages from selected intervals using cores C4 and C9 from this study, as well as cores from Collins et al. (2015; C3, C5, C6; 2015; Table 1).

Table 2
 ^{14}C activity of DIC in water column.

UCIAMS Lab ID	Water depth (m)	Fraction		$\Delta^{14}\text{C}$		^{14}C years	
		Modern	\pm	(‰)	\pm	(BP)	\pm
136749	12 m	0.8200	0.0017	–186.3	1.7	1595	20
136750	18 m	0.8180	0.0019	–188.3	1.9	1615	20
136751	28 m	0.2186	0.0022	–783.1	2.2	12210	90
136752	40 m	0.1964	0.0023	–805.1	2.3	13070	100
136753	45 m	0.1681	0.0024	–833.2	2.4	14330	120

3.2. Isotopic proxies: $^{87}\text{Sr}/^{86}\text{Sr}$, $\delta^{18}\text{O}$ and $\delta^{13}\text{C}$

The $^{87}\text{Sr}/^{86}\text{Sr}$ and $\delta^{13}\text{C}$ values from C4 (0–7000 cal yrs BP) and C9 (7900–8300 cal yrs BP) show a shift in aquifer hydrology sometime between 7000 and 8000 cal yrs BP (Tables 3 and 4; Fig. 11). The $^{87}\text{Sr}/^{86}\text{Sr}$ values in C9 from HN vary between 0.70840 and 0.70860 and the $\delta^{13}\text{C}$ values are between –5.0 and –8.0‰. C4 from IB has lower $^{87}\text{Sr}/^{86}\text{Sr}$ values ranging from 0.70820 to 0.70840 and the $\delta^{13}\text{C}$ values range from –11.3 to –11.6‰, but also have a decreasing trend with time (Fig. 11). Based on the Sr mixing relationship between fresh and marine water, this corresponds to a salinity shift of ~ 1.5–2.7 ppt in C9 to 1–1.5 ppt in C4. $\delta^{18}\text{O}$ values show little difference between C4 and C9, varying between –6.6 and –7.2‰ but are in the typical range for calcite in equilibrium with local freshwater (i.e. van Hengstum et al., 2009). As found in previous studies from coastal lagoons and estuaries, there is often a strong positive correlation between $^{87}\text{Sr}/^{86}\text{Sr}$ and $\delta^{13}\text{C}$, which is related to the mixing of fresh and marine waters. $\delta^{18}\text{O}$ values, however, do not always show a good relationship with $^{87}\text{Sr}/^{86}\text{Sr}$ for a variety of reasons (i.e. evaporation; Peros et al., 2007; Reinhardt et al., 2003).

3.3. Elemental proxies: Cl/Ca and Sr/Ca

The Cl/Ca and Sr/Ca records in C9 which are measured at 1 cm intervals show good correspondence with the intact C10 measured at 200 μm . Average Cl/Ca values for C9 and C10 are 0.016 (± 0.02 1σ) and 0.023 (± 0.02 1σ) while Sr/Ca is 0.061 (± 0.06 1σ) and 0.053 (± 0.05 1σ). The slight differences in the records can be attributed to the orientation of the rafts which are mostly flat-lying in the intact C10 versus the random orientation of calcite rafts in the sample reservoirs used for C9. In C10, measurements would be mostly cross-sectional as the core preserves its original depositional fabric,

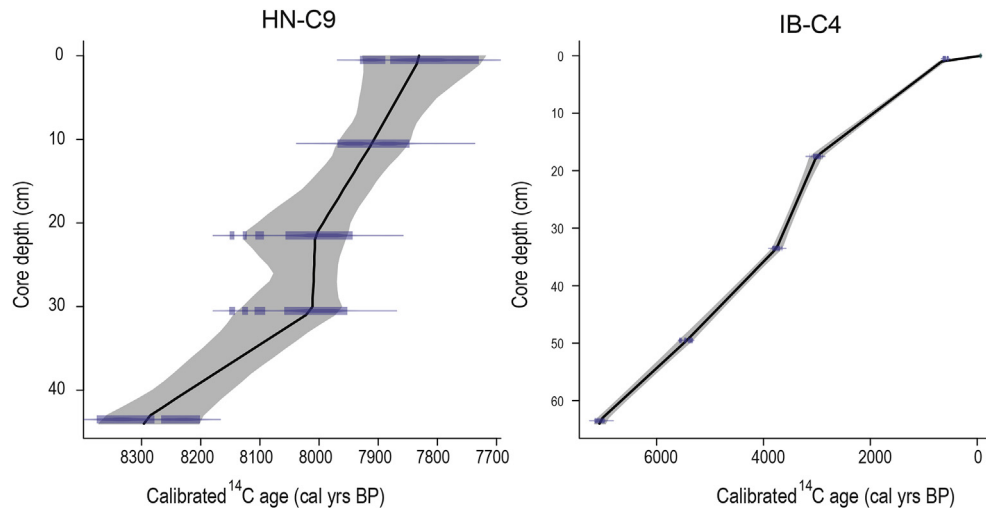


Fig. 9. Age Models of IB-C4 and HN-C9 using Clam 2.2 (Blaauw, 2010; Reimer et al., 2013). Grey shading represents calibrated age ranges (yrs BP) at 2σ confidence intervals.

while the samples loaded into reservoirs (C9) would include cross-sectional as well as surface area measurements (Fig. 10). There are also stratigraphic differences between C9 and C10 that are likely playing a role. Although C10 was collected in close proximity to C9, the point source of surface water agitation (i.e. drip water) may have moved slightly through time which could favor calcite raft deposition on one side of the pile versus another. Further research will be required to understand this process, but despite these minor differences, the average values for Cl/Ca and Sr/Ca for C9 and C10 are similar and are higher than those in C4 at $0.0011 (\pm 0.003 1\sigma)$ and $0.0041 (\pm 0.001 1\sigma)$ which is the most significant aspect in our analysis and discussion.

Sr/Ca ratios in abiotic calcite can be a reflection of temperature partitioning of Sr into the calcite crystal lattice, but in this instance, it is more likely a reflection of salinity and the mixing of fresh and marine water as the change is so large. The [Sr] in freshwater is lower (i.e. < 3 ppm; Reeve and Perry, 1994) than that of marine water (~ 8 ppm, Levinson, 1968) which is corroborated with our ceno measurements showing that the freshwater contains < 1.6 ppm [Sr] (Fig. 7).

The Cl/Ca records match the overall trend in Sr/Ca values (Fig. 11). Chlorine (Cl^-) behaves conservatively with the mixing of fresh and marine waters and its concentration is directly related to salinity (i.e. Perry et al., 2009). However, Cl^- is not partitioned into the calcite crystal lattice like other ions (i.e. Sr^{2+} , Mg^{2+} , Ba^{2+} ; Fairchild et al., 2001, 2006) and the samples were washed with deionized water to remove any pore water, so one would not expect to see trends in the data. Scanning Electron Microscope (SEM) analysis of the calcite rafts shows crystal rhombs extending down from the flat top of the raft (Fig. 5). The intersecting rhombs of calcite appear to be trapping fluid inclusions as the crystals coalesce and grow in size, so Cl/Ca would reflect changing meteoric WM salinity assuming the formation of fluid inclusions (i.e. volume) remained constant through time. This assumption seems to be valid at least in this case, as there is a very good relationship between Sr/Ca that is measured from the mineral phase and Cl/Ca that is from the fluid inclusions. If the volume of fluid inclusions varied through time we would not expect such a good relationship (Fig. 12). The slight spread in data is likely a result of minor changes in fluid inclusion volume but also variability in the [Sr] of the meteoric WM (i.e. weathering inputs of Sr^{2+}). In this study however, we place emphasis on the large difference in values between C4 and C9 rather than intra-core variation.

3.4. Diagenesis

There is no evidence indicating that the calcite raft material in C4 and C9 has been diagenetically altered (also C10). There are no cemented layers and SEM analysis of the calcite rafts shows that they retain their original crystal fabric with no overgrowths or pitting (i.e. secondary alteration effects; Figs. 5 and 10). Calcite rafts form through the addition of down- and out-ward precipitating crystal rhombs which form a flat top at the air water interface. Diagenetic calcite overgrowths would form on all surfaces, but we observed no rhombs on the flat, upper portion of the rafts (Fig. 5). As discussed previously, there is also close agreement between the isotopic ($\delta^{13}\text{C}$, $^{87}\text{Sr}/^{86}\text{Sr}$) and elemental (Cl/Ca, Sr/Ca) proxies, although the $\delta^{18}\text{O}$ values did not show a significant change through time. In terms of diagenesis, the similarity in $\delta^{18}\text{O}$ values from C4 and C9 is worth noting, as we might expect $\delta^{18}\text{O}$ values in C9 to be affected by sea water (i.e. $\delta^{18}\text{O} \sim 0\text{‰}$) as it was immersed in the marine WM with Holocene sea-level rise.

4. Discussion

4.1. Water level and calcite raft distribution in HN and IB

The sedimentary and micropaleontological evidence indicates that there was water at the bottom of HN by at least ~ 10 ca kyrs BP which is a good fit with Holocene sea-level records, but skeletal taphonomy is consistent with the presence of water at the bottom of the pit prior to that date (–42 m, Fig. 4; Collins et al., 2015; Chatters et al., 2014). Collins et al. (2015) speculated that there may have been an underlying aquitard, allowing “ponding” of water raising water levels during large rainfalls in HN. These were likely shortterm events and are evidenced by the depth distribution of skeletal elements, and ^{14}C dates from OM on ledges in HN. However, shortterm sea-level oscillations may also be raising water levels in HN as evidenced during the mid-late Holocene from a speleothem in a nearby cave (Balam Can Chee) in the Sac Actun cave System (1.6 kms from the coast; Moseley et al., 2015).

Calcite raft formation would not begin until groundwater level rose permanently flooding the bottom of HN after ~ 10 cal kyrs BP; however, calcite rafts in C9 didn't begin to accumulate until much later (7900–8300 cal yrs BP). There is no direct data for water level between 8 and 10 cal kyrs BP, but groundwater reaches the floor of the upper cave passages by ~ 8000 cal yrs BP (~ –12 m) based on the

Table 3
IB-C4 Geochemical data.

Core Depth (cm)	Cl/Ca	Sr/Ca	$\delta^{13}\text{C}$ (‰)	$\delta^{18}\text{O}$ (‰)	$^{87}\text{Sr}/^{86}\text{Sr}$
0.5	0.0020	0.0036			
1.5	0.0010	0.0034	–11.7	–6.4	0.70839
2.5	0.0011	0.0034			
3.5	0.0010	0.0034	–11.4	–6.4	
4.5	0.0011	0.0035			
5.5	0.0009	0.0030	–11.5	–6.5	0.70828
6.5	0.0009	0.0025			
7.5	0.0009	0.0028	–11.5	–6.6	
8.5	0.0009	0.0032			
9.5	0.0007	0.0029	–11.4	–6.5	0.70836
10.5	0.0009	0.0032			
11.5	0.0009	0.0030	–11.4	–6.4	
12.5	0.0010	0.0033			
13.5	0.0009	0.0035	–11.3	–6.3	
14.5	0.0009	0.0035			
15.5	0.0011	0.0038	–11.3	–6.3	
16.5	0.0012	0.0037			
17.5	0.0012	0.0038	–11.3	–6.3	0.70832
18.5	0.0008	0.0040			
19.5	0.0008	0.0034	–11.4	–6.5	
20.5	0.0011	0.0036			
21.5	0.0011	0.0034	–11.3	–6.4	
22.5	0.0011	0.0037			
23.5	0.0009	0.0035	–11.2	–6.3	
24.5	0.0013	0.0043			
25.5	0.0011	0.0038	–11.4	–6.4	0.70830
26.5	0.0007	0.0026			
27.5	0.0007	0.0025	–11.4	–6.5	
28.5	0.0006	0.0026			
29.5	0.0007	0.0026	–11.4	–6.5	
30.5	0.0005	0.0025			
31.5	0.0007	0.0026	–11.4	–6.3	
32.5	0.0010	0.0036			
33.5	0.0010	0.0040	–11.3	–6.4	
34.5	0.0011	0.0035			
35.5	0.0008	0.0029	–11.4	–6.4	
36.5	0.0009	0.0030			
37.5	0.0008	0.0027	–11.4	–6.6	
38.5	0.0010	0.0039			
39.5	0.0011	0.0043	–11.4	–6.7	
40.5	0.0010	0.0034			
41.5	0.0009	0.0035	–11.5	–6.6	0.70830
42.5	0.0013	0.0045			
43.5	0.0008	0.0034	–11.5	–6.7	
44.5	0.0009	0.0039			
45.5	0.0010	0.0045	–11.4	–6.6	0.70828
46.5	0.0009	0.0035			
47.5	0.0009	0.0036	–11.4	–6.8	
48.5	0.0010	0.0038			
49.5	0.0011	0.0042	–11.3	–6.4	0.70832
50.5	0.0013	0.0061			
51.5	0.0011	0.0046	–11.1	–6.3	
52.5	0.0013	0.0058			
53.5	0.0014	0.0058	–11.2	–6.5	0.70827
54.5	0.0013	0.0050			
55.5	0.0015	0.0065	–11.5	–6.5	
56.5	0.0017	0.0062			
57.5	0.0017	0.0070	–11.4	–6.8	0.70820
58.5	0.0016	0.0061			
59.5	0.0022	0.0075	–11.3	–6.5	
60.5	0.0016	0.0068			
61.5	0.0013	0.0071	–11.1	–6.7	
62.5	0.0015	0.0074	–11.2	–6.7	
63.5	0.0016	0.0074	–11.3	–7.0	
64.5	0.0013	0.0077			

Table 4
HN-C9 Geochemical data.

Core Depth (cm)	Cl/Ca	Sr/Ca	$\delta^{13}\text{C}$ (‰)	$\delta^{18}\text{O}$ (‰)	$^{87}\text{Sr}/^{86}\text{Sr}$
0.5	0.014	0.029	–8.0	–6.9	0.70847
1.5	0.008	0.030			
2.5	0.009	0.030	–7.1	–6.4	
3.5	0.023	0.044			
4.5	0.021	0.043			
5.5	0.015	0.038	–6.2	–6.2	0.70847
6.5	0.011	0.038			
7.5	0.019	0.053	–6.1	–6.4	
8.5	0.014	0.048			
9.5	0.025	0.067			
10.5	0.023	0.061	–6.2	–6.6	0.70851
11.5	0.034	0.071			
12.5	0.050	0.089	–7.0	–6.3	
13.5	0.037	0.072			
14.5	0.041	0.073			
15.5	0.025	0.058	–6.3	–6.5	0.70852
16.5	0.019	0.076			
17.5	0.020	0.060	–7.3	–6.6	
18.5	0.020	0.059			
19.5	0.020	0.057	–6.8	–6.3	
20.5	0.022	0.054			
21.5	0.020	0.060	–6.5	–6.4	0.70843
22.5	0.039	0.085	–5.8	–6.3	
23.5	0.044	0.090			
24.5	0.034	0.080			
25.5	0.014	0.045	–6.3	–6.5	0.70842
26.5	0.016	0.050			
27.5	0.015	0.038	–5.4	–6.4	
28.5	0.011	0.031			
29.5	0.025	0.044			
30.5	0.026	0.045	–6.3	–6.7	0.70842
31.5	0.027	0.051			
32.5	0.032	0.052	–6.5	–6.8	
33.5	0.022	0.044			
34.5	0.017	0.038			
35.5	0.040	0.049	–5.6	–6.5	0.70847
36.5	0.020	0.043			
37.5	0.021	0.033	–6.4	–6.7	
38.5	0.012	0.029			
39.5	0.019	0.033			
40.5	0.006	0.014	–5.5	–6.7	
41.5	0.008	0.009			
42.5	0.003	0.007			
43.5	0.010	0.008	–7.0	–6.5	0.70847
44.5	0.014	0.011			

column. Calcite raft formations have not been studied in the Yucatán, and we only have observations from shallow water depths (i.e. <10 m) with no deep water examples to provide a basis for assessment. However, a 30 m water column seems large for the formation of such a distinctive, cone-shaped raft pile. It could be that this location had a vigorous point-source of water agitation (i.e. drip water) creating a concentrated stream of calcite rafts settling through the water column that was active over a short time-period which would explain the high sediment accumulation rate in C9 (~ 0.11 cm/yr). More research is required from analogous environments, but regardless of the water depth in HN, the calcite rafts formed at the air/water interface as water level was rising in the pit, but was below the base of the upper cave passages (–12 m).

In IB, calcite rafts formed large accumulations as groundwater level rise decelerated in the mid-Holocene. In IB, they are covering the breakdown pile to the extent that many of the limestone boulders are buried under calcite rafts and OM with no recognizable cone-shaped piles (see Collins et al., 2015 for details on stratigraphy). The more extensive calcite raft coverage might be due to the deceleration of sea-level rise over the past 7 cal kyrs BP coupled with a drier climate, which would allow for prolonged periods of supersaturation of CaCO_3 in the upper meteoric WM (Taylor and

IB core stratigraphy (Collins et al., 2015). There is considerable uncertainty on sea-level position from 8 to 10 cal kyrs BP, but using the sea-level curve and the date for the flooding of the upper cave passage as a guide, the water level in HN was anywhere from ~ –12 to –30 msl when the raft pile formed (Fig. 4; C9; Moseley et al., 2015). This would be equivalent to a ~ 15–30 m thick water

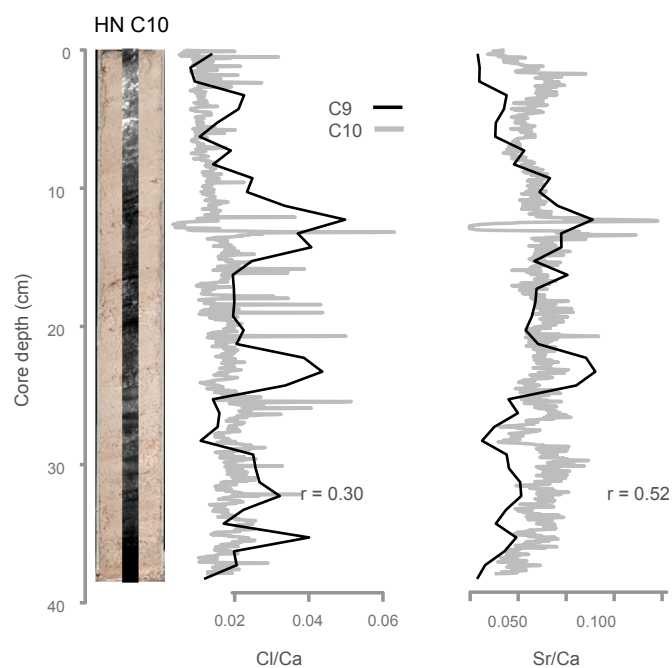


Fig. 10. Correlation between Cl/Ca and Sr/Ca data in C9 and C10. C9 was analyzed at 1 cm resolution vs C10 which was intact and measured at 200 μm . Correlation coefficients (r -value) between C9 and C10 records are also shown. The optical and radiographic image of C10 shows slightly inclined bedding and laminae which is due to calcite rafts accumulating from a point source and forming a cone-shaped pile. There were no cemented or indurated layers within the core.

Chafetz, 2004). Kovacs et al. (2017b) found seasonal trends (wet vs. dry) in the formation of calcite rafts in modern-day localities, with large rainfalls diluting CaCO_3 saturated surface water hindering calcite raft formation for short periods of time. Further research is required to determine whether this dilution effect is scalable and applicable to long-term trends.

4.2. Aquifer salinity and relationship with wet and dry periods

4.2.1. Consistency between geochemical proxies

The isotopic and elemental proxies show a consistent pattern of change between C9 and C4 indicative of a change in the salinity of the meteoric WM. Calcite raft geochemistry shows a marked shift as groundwater floods the upper cave passages at ~ 8000 cal yrs BP (Collins et al., 2015). C9 from HN provides a short record of the meteoric WM (7900–8300 cal yrs BP) and the data differs in terms of magnitude and variability relative to that of C4 in IB, which spans a longer period of time (\sim last 7000 cal yrs BP). The values of $^{87}\text{Sr}/^{86}\text{Sr}$, Cl/Ca, Sr/Ca and $\delta^{13}\text{C}$ show the largest changes, whereas $\delta^{18}\text{O}$ shows little change between the cores.

The Sr isotopes indicate a negative (1–3 ppt) shift in meteoric WM salinity between C9 and C4 but this maybe an underestimate of the salinity change, as our mixing equation assumes that the $^{87}\text{Sr}/^{86}\text{Sr}$ value of freshwater is similar to that of present day. When groundwater level was lower and dissolving older limestone, the $^{87}\text{Sr}/^{86}\text{Sr}$ of the freshwater end-member may have been lower than present values which would result in a higher salinity estimate for C9 relative to C4 (i.e. $^{87}\text{Sr}/^{86}\text{Sr} = 0.7082$; McArthur et al., 2001). The $\delta^{13}\text{C}$ record also shows a similar shift in salinity; however, the shift in $\delta^{13}\text{C}$ from C9 to C4 is large ($\sim -5\%$) relative to the estimated change of 1–3 ppt and must be due to other factors affecting $\delta^{13}\text{C}$ of the DIC composition (e.g., our salinity estimates; composition of surficial vegetation; e.g. Peros et al., 2007; Pohlman et al., 1997).

Similarly, Cl/Ca and Sr/Ca show a large change from C9 to C4, which is consistent with a decrease in salinity, as concentrations of Cl^- and Sr^{2+} are lower in fresh water than in marine water (Perry et al., 2009). Seawater (~ 35 ppt) has an approximate Cl^- concentration of 19 400 mg/l while freshwater (0.001–0.5 ppt) typically ranges from 1 to 250 mg/L. Therefore, the decrease in Cl/Ca between C9 and C4 is consistent with the 3 ppt salinity change (~ 1500 mg/L Cl^-), assuming the freshwater end-member is < 100 mg/L. The Cl/Ca ratio is 10–20 times higher in C9 relative to C4 in IB where the modern salinity is 1.1 ppt (Figs. 3 and 11). Further research is required to calibrate the relationship between Cl/Ca and salinity to be definitive, but the evidence does indicate a shift in salinity between C9 and C4, which is corroborated with some of the isotopic data.

In contrast, the $\delta^{18}\text{O}$ values, only show a minor difference between C9 and C4, with values ranging from -7.2 to -6.6% in both cores. $\delta^{18}\text{O}$ values, alone, are not always useful for salinity reconstructions in coastal environments (e.g. Peros et al., 2007). As will be discussed, aquifer hydrology over wet/dry periods is likely obscuring the effect of salinity shift on the $\delta^{18}\text{O}$ values.

4.2.2. Hydrological implications

Previous studies have shown Holocene changes in annual precipitation linked with the migration of the ITCZ (i.e. Hodell et al., 2005; Metcalfe et al., 2000). Haug et al. (2001) used Ti records from laminated sediments from the Cariaco basin near Venezuela to show dry conditions during the Younger Dryas (~ 11 – 13 cal kyrs BP) and then a rapid rise in moisture between 11 and 10 cal kyrs BP. Levels then peak at 9 cal kyrs BP, followed by a gradual drying trend to present. Further to the north, the $\delta^{18}\text{O}$ record from ostracod shells (*Candona* sp.) in Lake Miragoâne, Haiti shows dry conditions at ~ 12 cal kyrs BP and then increasing moisture to ~ 7 cal kyrs BP and then a gradual drying to present (Curtis and Hodell, 1993; Hillesheim et al., 2005; Hodell et al., 1991). Based on the calcite raft geochemistry, the aquifer was more saline (>1 – 3 ppt) during wetter conditions at 7.9–8.3 cal kyrs BP than it was after 7 cal kyrs BP, when climate conditions were becoming more arid (1–2 ppt). The salinity change likely reflects, in part, a change in hydrology associated with decreasing flow in the meteoric WM.

We can understand this seeming contradictory relationship, by consideration of measurements of modern cave waters during times of intense precipitation. Recent instrumental monitoring of meteoric WM salinity (~ 4 yrs) shows that intense rainfalls (i.e. hurricanes and tropical depressions) cause turbulent mixing between it, and the underlying marine WM increasing its salinity (a change from 6 ppt to > 9 ppt; Coutino et al., 2017; Kovacs et al., 2017a). Kovacs et al. (2017b) found a similar relationship between salinity and rainfall in cenote surface waters. Assuming that it is a scalable effect, during drier periods, the meteoric WM might be thinner, but less saline, due to less frequent and intense rainfall events.

There are however, likely other factors affecting the salinity of the meteoric WM. The shift in salinity between C9 (HN) and C4 (IB) is sudden and relatively large, suggesting a rapid change of state in the hydrology. This sudden change in meteoric WM salinity corresponds to water level rise and flooding of the upper cave passages (~ 12 m). Regionally, this is the approximate depth for most of the explored cave passages in Quintana Roo which are large anastomosing systems that are interconnected. There is little information on the early hydrological regime (e.g. stratification) when groundwater levels were lower, but the lack of cave passages in the older, deeper limestone (i.e., mega-porosity) suggests that the hydrology may have been quite different than present. The presence of abundant detrital OM scattered at the bottom of HN and on ledges which originated from cenote openings (eg. IB, La Concha),

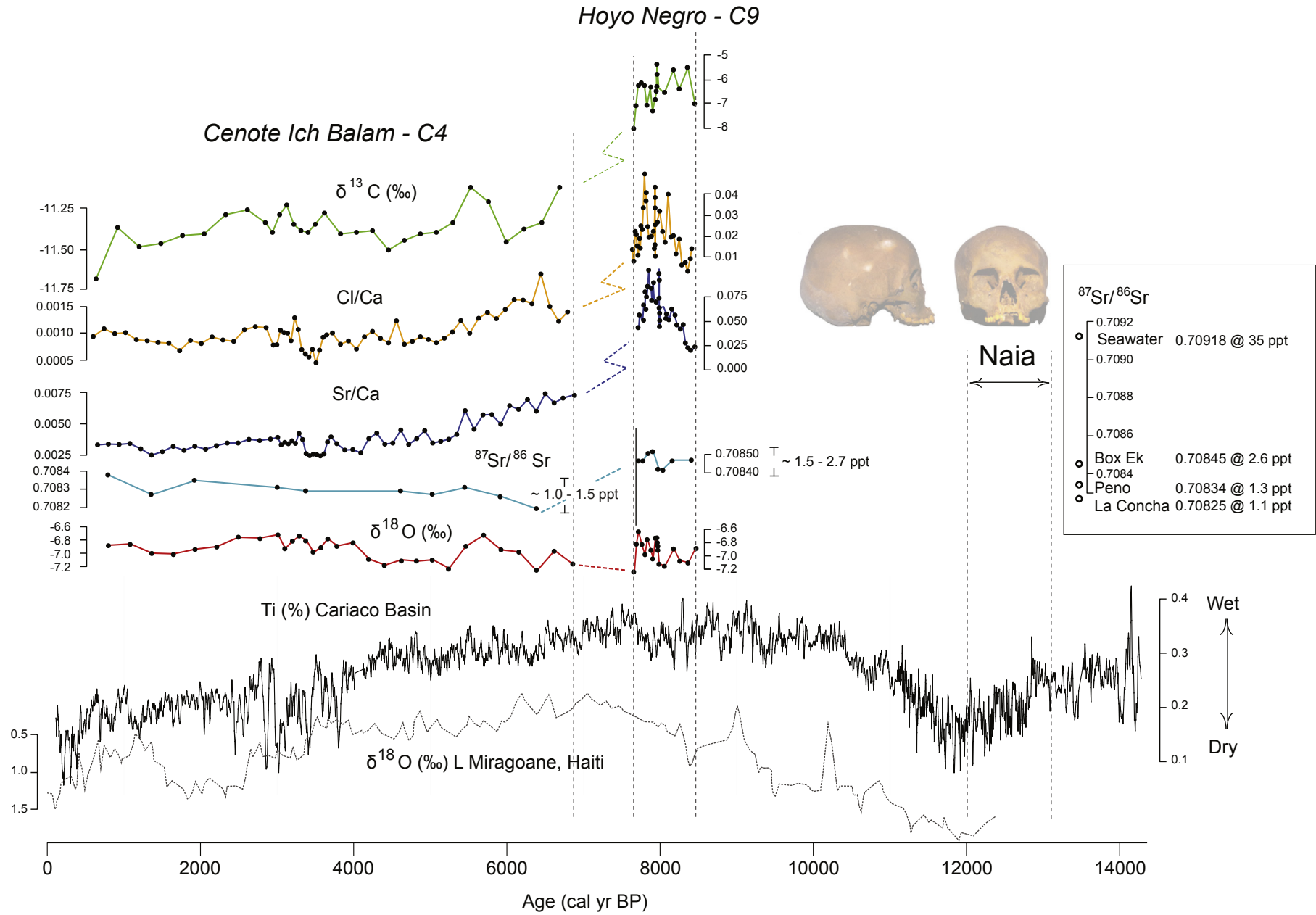


Fig. 11. Geochemical data for IB and HN plotted vs age (note different scales for C4 and C9) and comparisons with the (Ti) record from the Cariaco Basin (see Fig. 1 for geographical position; Haug et al., 2001) and Lake Miragoane in Haiti (Hodell et al., 1991). Inset figure provides reference to $^{87}\text{Sr}/^{86}\text{Sr}$ and salinity based on measured values.

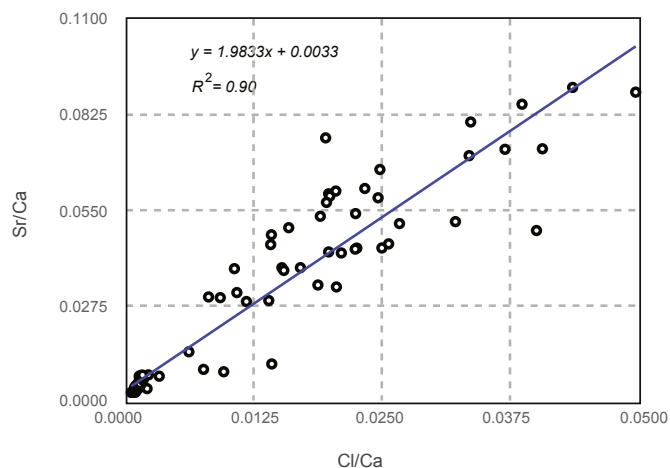


Fig. 12. Crossplot showing the direct relationship between Cl/Ca and Sr/Ca. Data includes C4 and C9.

suggests precipitation induced flows in the upper cave passages that emptied into HN and may have caused increased turbulent mixing with the underlying marine WM. Because of the ~ 1 Ka gap in the depositional sequence, we have no record of the transition when water levels rose and flooded the upper passages, but the change in hydrological regime does appear to have occurred quickly, suggested by the large change in salinity between C9 and C4. Further research is needed, but the flooding of shallow cave passages with Holocene sea-level rise, in addition to climatic change, may have influenced aquifer hydrology.

The salinity records from IB show a gradual decrease associated with the increase in aridity since the mid-Holocene as documented in Lake Miragoane and the Cariaco Basin. In a nearby but separate cave system (Aktun Ha) microfossils, (thecamoebians and foraminifera) also show a gradual decrease in meteoric WM salinity over the past 7 Ka demonstrating that the aquifer is responding on a regional basis to climate trends but also perhaps to deceleration of sea-level since ~ 6 ks BP (e.g. coastal plugging with shoreline progradation; van Hengstum et al., 2010).

As discussed, $\delta^{18}\text{O}$ values show little change over the past 8.3 cal kyrs BP, unlike the other geochemical data. However, they do corroborate with other records when the $\delta^{18}\text{O}$ change in precipitation is considered over wet and dry periods. Based on the data from the stalagmite (“Chaac”) collected from the Tzabnah (Tecoh) Cave in the northern Yucatán (20° 45'N, 89° 28'W; 20 m above sea level), $\delta^{18}\text{O}$ values are ~ 3‰ higher during dry periods (–3.4‰) than during wet ones (–6.4‰; Medina-Elizalde et al., 2010). So during wet periods, the $\delta^{18}\text{O}$ of the meteoric WM would be expected to be isotopically lighter (i.e. ~ –6‰), but increased mixing with the underlying marine water ($\delta^{18}\text{O}$ values ~ 0‰) would counter that change. During dry periods, the meteoric WM would be less saline, so $\delta^{18}\text{O}$ values would be closer to the precipitation value of ~ –3‰. Thus, over wet and dry periods there would be little change in $\delta^{18}\text{O}$ values which is what we document in our data.

4.2.3. Implications for the early Holocene aquifer

The results from IB and HN demonstrate that the inter-relationship among aquifer salinity (i.e. potability), precipitation and cave geomorphology is complex and not necessarily predictable with the present state of knowledge. More paleo-hydrological data from the early Holocene is required to be definitive, but our results from HN present important questions on early Paleoamerican subsistence in the Yucatan. Based on the Cariaco runoff proxy, elemental titanium (Ti) records indicate that regional climates in

the Caribbean would have been relatively dry during the Younger Dryas (c. 12 900 to c. 11 700 cal yrs BP; Haug et al., 2001). This aridity coupled with lower groundwater levels would have limited the extent and accessibility of surficial water (e.g. lakes), and if as predicted, groundwater was potable, it would have been the only year-round water source other than small cave pools which would not be large or abundant (e.g. rimstone dams). Most of the explored cave passages in Quintana Roo are shallow (~ –10 to –12 m) with few known deep passages or caverns in the vicinity of HN to access groundwater (i.e. Fig. 2; The Pit, Cenote Angelita; Quintana Roo Speleological Survey, 2017). If our arguments hold true, early Paleoamericans would not be able to range extensively and movements would need to be carefully planned especially in the dry-season.

5. Conclusions

This study shows for the first time that geochemical records from calcite raft deposits can be used as a proxy for paleohydrological conditions. Calcite rafts record aquifer chemistry as they precipitate at the air-water interface and form large and spatially extensive accumulations in Yucatán caves. The geochemical records ($^{87}\text{Sr}/^{86}\text{Sr}$, Cl/Ca, Sr/Ca and $\delta^{13}\text{C}$) from IB and HN show similar trends in aquifer salinity with the Cl/Ca records showing the most promise in terms of understanding groundwater hydrology. Analyzing intact cores with the efficiencies of XRF core scanners (i.e. ITRAX) will provide increased temporal resolution and spatial extent.

The hydrology of the aquifer also seems to be responding to regional climate with wet periods having higher meteoric WM salinity vs. drier intervals where it is less saline. It is unclear how the aquifer was affected by cave geomorphology, but it seems likely that Holocene sea-level rise is having an effect with the flooding of the extensive shallow cave passages in the Yucatán. Further research will extend the spatial and temporal data to determine variability in the aquifer response which may prove useful for predicting future trends with climate and sea-level change. However, our results from HN and Cenote Ich Balam (IB) show that calcite raft deposits have potential as a paleohydrological archive for the Yucatan, but also for karst aquifers world-wide.

Acknowledgments

The authors would like to acknowledge and thank Dr. Todd Kincaid (Geohydros LLC) and the anonymous reviewers for comments which improved the manuscript. Martin Knyf and Dr. Alan Dickin provided assistance in isotopic analysis. We are grateful to the numerous volunteers, especially Alex Alvarez, Ali Perkins and Cameron Russo, who have contributed with cave surveying and sample retrieval as well as Roberto Chavez for photography. We also appreciate the assistance of Zero Gravity Dive Center and ProTec Dive Center Tulum, as well as the generosity of Marcia Kirby. Financial support for the project was provided through NSERC Discovery Grants (EGR - 2015-05725 and STK - 386188-2010), CFI-JELF (EGR - 31962), NSERC CGSD (SEK), Geological Society of America Graduate Student Research Grants (SEK), National Geographic Expeditions Council (JCC, DR, EGR and ANB) and the Instituto Nacional de Antropología e Historia (INAH). Research in Hoyo Negro is conducted under the auspices of the Subdirección de Arqueología Subacuática de INAH, and with the permission of the Consejo de Arqueología del INAH. We would especially like to thank Adriana Velázquez Morlet, Director of INAH's Center in Quintana Roo.

References

- Bard, E., Hamelin, B., Arnold, M., Montaggioni, L., Cabioch, G., Faure, G., Rougerie, F., 1996. Deglacial sea-level record from Tahiti corals and the timing of global meltwater discharge. *Nature* 382, 241–244. <https://doi.org/10.1038/382241a0>.
- Bard, E., Hamelin, B., Delanghe-Sabatier, D., 2010. Deglacial meltwater pulse 1B and Younger Dryas sea levels revisited with boreholes at Tahiti. *Science* 327, 1235–1237. <https://doi.org/10.1126/science.1180557>.
- Bauer-Gottwein, P., Gondwe, B.R.N., Charvet, G., Marin, L.E., Rebolledo-Vieyra, M., Merediz-Alonso, G., 2011. Review; the Yucatan Peninsula karst aquifer, Mexico. *Hydrogeol. J.* 19, 507–524. <https://doi.org/10.1007/s10040-010-0699-5>.
- Bautista, F., Palacio-Aponte, G., Quintana, P., Zinck, J.A., 2011. Spatial distribution and development of soils in tropical karst areas from the Peninsula of Yucatan, Mexico. *Geomorphology* 135, 308–321. <https://doi.org/10.1016/j.geomorph.2011.02.014>.
- Beddows, P.A., 2004. Groundwater Hydrology of a Coastal Conduit Carbonate Aquifer: Caribbean Coast of the Yucatan Peninsula. Mexico Unpublished doctoral dissertation. University of Bristol.
- Beddows, P.A., Smart, P.L., Whitaker, F.F., Smith, S.L., 2007. Decoupled fresh–saline groundwater circulation of a coastal carbonate aquifer: spatial patterns of temperature and specific electrical conductivity. *J. Hydrol* 346 (1–2), 18–32. <https://doi.org/10.1016/j.jhydrol.2007.08.013>.
- Blaauw, M., 2010. Methods and code for “classical” age-modelling of radiocarbon sequences. *Quat. Geochronol.* 5, 512–518. <https://doi.org/10.1016/j.quageo.2010.01.002>.
- Blanchon, P., 2005. Comments on “Corrected western Atlantic sea-level curve for the last 11,000 years based on calibrated ¹⁴C dates from *Acropora palmata* framework and intertidal mangrove peat” by Toscano and Macintyre [Coral Reefs (2003) 22:257–270]. *Coral Reefs* 24, 183–186. <https://doi.org/10.1007/s00338-004-0472-0>.
- Blanchon, P., Jones, B., Ford, D.C., 2002. Discovery of a submerged relic reef and shoreline off Grand Cayman: further support for an early Holocene jump in sea level. *Sediment. Geol.* 147, 253–270. [https://doi.org/10.1016/S0037-0738\(01\)00143-9](https://doi.org/10.1016/S0037-0738(01)00143-9).
- Blanchon, P., Shaw, J., 1995. Reef drowning during the last deglaciation: evidence for catastrophic sea-level rise and ice-sheet collapse. *Geology* 23, 4–8. [https://doi.org/10.1130/0091-7613\(1995\)023<0004:RDDTLD>2.3.CO](https://doi.org/10.1130/0091-7613(1995)023<0004:RDDTLD>2.3.CO).
- Bryant, J.D., Jones, D.S., Mueller, P.A., 1995. Influence of freshwater flux on ⁸⁷Sr/⁸⁶Sr chronostratigraphy in marginal marine environments and dating of vertebrate and invertebrate faunas. *J. Paleontol.* 69, 1–6.
- Chagué-Goff, C., Chan, J.C.H., Goff, J., Gadd, P., 2016. Late Holocene record of environmental changes, cyclones and tsunamis in a coastal lake, Mangaia, Cook Islands. *Isl. Arc* 25, 333–349. <https://doi.org/10.1111/iar.12153>.
- Chatters, J.C., Kennett, D.J., Asmerom, Y., Kemp, B.M., Polyak, V., Nava-Blank, A., Beddows, P.A., Reinhardt, E., Arroyo-Cabrales, J., Bolnick, D.A., Malhi, R.S., Culleton, B.J., Luna-Erreguerena, P., Rissolo, D., Morell-Hart, S., Stafford, T.W., 2014. Late Pleistocene human skeleton and mtDNA link Paleoamericans and modern Native Americans. *Sci.* (80) 344, 750–754. <https://doi.org/10.1126/science.1252619>.
- Chatters, J.C., Rissolo, D., Arroyo-Cabrales, J., Stafford Jr., T.W., Kemp, B.M., Alvarez, A., Nava-Blank, A., Attolini, F., Beddows, P.A., Reinhardt, E., Kovacs, S., Collins, S., Morell-Hart, S., Chávez-Arce, R., Bird, S., Luna Erreguerena, P., 2017. Hoyo Negro: tapping the paleoanthropological and paleoecological potential of a deeply submerged, underground chamber on the Yucatan Peninsula, Mexico. In: *The Archaeology of Underwater Caves*. Oxbow Books, Oxford, pp. 119–129.
- Collins, S.V., Reinhardt, E.G., Rissolo, D., Chatters, J.C., Nava Blank, A., Luna Erreguerena, P., 2015. Reconstructing water level in Hoyo Negro, Quintana Roo, Mexico, implications for early Paleoamerican and faunal access. *Quat. Sci. Rev.* 124, 68–83. <https://doi.org/10.1016/j.quascirev.2015.06.024>.
- Coutino, A., Stastna, M., Kovacs, S., Reinhardt, E., 2017. Hurricanes Ingrid and Manuel (2013) and their impact on the salinity of the Meteoric Water Mass, Quintana Roo, Mexico. *J. Hydrol.* 551, 715–729. <https://doi.org/10.1016/j.jhydrol.2017.04.022>.
- Curtis, J.H., Hodell, D.A., 1993. An isotopic and trace element study of ostracods from Lake Miragoane, Haiti: a 10,500 year record of paleosalinity and paleotemperature changes in the Caribbean. *Clim. Chang. Cont. Isot. Rec.* 135–152.
- Curtis, J.H., Hodell, D.A., Brenner, M., 1996. Climate variability on the Yucatan Peninsula (Mexico) during the past 3500 Years, and implications for Maya cultural evolution. *Quat. Res.* 47, 37–47. <https://doi.org/10.1006/qres.1996.0042>.
- Fairbanks, R.G., 1989. A 17,000-year glacio-eustatic sea level record: influence of glacial melting rates on the Younger Dryas event and deep-ocean circulation. *Nature* 342, 637–642.
- Fairchild, I.J., Baker, A., Borsato, A., Frisia, S., Hinton, R.W., McDermott, F., Tooth, A.F., 2001. Annual to sub-annual resolution of multiple trace-element trends in speleothems. *J. Geol. Soc. Lond.* 158, 831–841.
- Fairchild, I.J., Smith, C.L., Baker, A., Fuller, L., Spötl, C., Matthey, D., McDermott, F., 2006. Modification and preservation of environmental signals in speleothems. *Earth Sci. Rev.* 75, 105–153.
- Fornós, J.J., Ginés, J., Gracia, F., 2009. Present-day sedimentary facies in the coastal karst caves of Mallorca Island (western Mediterranean). *J. Cave Karst Stud.* 71, 86–99.
- Gabriel, J.J., Reinhardt, E.G., van Hengstum, P.J., Beddows, P.A., Peros, M.C., Davidson, D.E., 2009. Palaeoenvironmental evolution of Cenote Aktun Ha (Carwash) on the Yucatan Peninsula, Mexico and its response to Holocene sea-level rise. *J. Paleolimnol.* 42, 199–213. <https://doi.org/10.1007/s10933-008-9271-x>.
- Gázquez, F., Calaforra, J.M., 2013. Origin of double-tower raft cones in hypogenic caves. *Earth Surf. Process. Landforms* 38, 1655–1661. <https://doi.org/10.1002/esp.3399>.
- González-Herrera, R., Sánchez-y-Pinto, I., Gamboa-Vargas, J., 2002. Groundwater-flow modeling in the Yucatan karstic aquifer, Mexico. *Hydrogeol. J.* 10, 539–552. <https://doi.org/10.1007/s10040-002-0216-6>.
- González, A.H., Terrazas, A., Stinnesbeck, W., Benavente, M.E., Avilés, J., Rojas, C., Padilla, J.M., Velásquez, A., Acevez, E., Frey, E., 2013. The First Human Settlers on the Yucatan Peninsula: Evidence from Drowned Caves in the State of Quintana Roo, Mexico. *Paleoamerican Odyssey*, pp. 323–337.
- González González, A.H., Sandoval, C.R., Acevez Nunez, E., Olguin, J., Ramirez, S.A., del Rio Lara, O., Erreguerena, P.L., Velazquez Morlet, A., Stinnesbeck, W., Terrazas Mata, A., Benavente Sanvicente, M., 2016. Underwater and Maritime Archaeology in Latin America and the Caribbean, 2nd ed., Evidence of Early Inhabitants in Submerged Caves in Yucatan, Mexico. Routledge, New York, pp. 127–142.
- González González, A.H., Sandoval, C.R., Mata, A.T., Sanvicente, M.B., Stinnesbeck, W., O, J.A., De, M., 2008. The arrival of humans on the Yucatan Peninsula: evidence from submerged caves in the state of Quintana Roo, Mexico. *Curr. Res. Pleistocene* 25, 1–24.
- Gregory, B.R.B., Reinhardt, E.G., Macumber, A.L., Nasser, N.A., Patterson, R.T., Kovacs, S.E., Galloway, J.M., 2017. Sequential sample reservoirs for Itrax-XRF analysis of discrete samples. *J. Paleolimnol.* 57, 287–293. <https://doi.org/10.1007/s10933-017-9944-4>.
- Hastenrath, S., 2012. *Climate Dynamics of the Tropics*, 8th ed. Springer Science & Business Media.
- Haug, G.H., Hughen, K.A., Sigman, D.M., Peterson, L.C., Röhl, U., Peterson, L.C., Overpeck, J.T., Kipp, N.G., Imbrie, J., Hughen, K.A., Overpeck, J.T., Peterson, L.C., Trumbore, S.E., Peterson, L.C., Haug, G.H., Hughen, K.A., Röhl, U., Hastenrath, S., Greishar, L., Röhl, U., Abrams, L.J., Yarinck, K.M., Murray, R.W., Peterson, L.C., Members, C., Hammen, T., van der Hooghiemstra, H., deMenocal, P., Ortiz, J., Guilderson, T., Sarnthein, M., Fairbanks, R.G., Mayle, F.E., Burbridge, R., Killeen, T.J., Berger, A., Loutre, M.F., Maslin, M.A., Burns, S.J., Fedorov, A.V., Philander, S.G., Clement, A.C., Seager, R., Cane, M.A., Peterson, M.J., Chang, P., Ji, L., Li, H., Hodell, D.A., Brenner, M., Curtis, J.H., Guilderson, T., Cane, M., Clement, A.C., 2001. Southward migration of the intertropical convergence zone through the Holocene. *Science* 293, 1304–1308. <https://doi.org/10.1126/science.1059725>.
- Hill, C.A., Forti, P., 1997. *Cave Minerals of the World*, 2nd ed. National Speleological Society, Huntsville, Ala.
- Hillesheim, M.B., Hodell, D.A., Leyden, B.W., Brenner, M., Curtis, J.H., Anselmetti, F.S., Ariztegui, D., Buck, D.G., Guilderson, T.P., Rosenmeier, M.F., 2005. Climate change in lowland Central America during the late deglacial and early Holocene. *J. Quat. Sci.* 20, 363–376.
- Hodell, D.A., Brenner, M., Curtis, J.H., 2007. Climate and cultural history of the northeastern Yucatan Peninsula, Quintana Roo, Mexico. *Clim. Change* 83, 215–240. <https://doi.org/10.1007/s10584-006-9177-4>.
- Hodell, D.A., Brenner, M., Curtis, J.H., 2005. Terminal Classic drought in the northern Maya lowlands inferred from multiple sediment cores in Lake Chichancanab (Mexico). *Quat. Sci. Rev.* 24, 1413–1427. <https://doi.org/10.1016/j.quascirev.2004.10.013>.
- Hodell, D.A., Curtis, J.H., Jones, G.A., Higuera-Gundy, A., Brenner, M., Binford, M.M., Dorsey, K.T., 1991. Reconstruction of Caribbean climate change over the past 10,500 years. *Nature* 352, 790–793. <https://doi.org/10.1038/352790a0>.
- Hodell, D.A., Quinn, R.L., Brenner, M., Kamenov, G., 2004. Spatial variation of strontium isotopes (⁸⁷Sr/⁸⁶Sr) in the Maya region: a tool for tracking ancient human migration. *J. Archaeol. Sci.* 31, 585–601. <https://doi.org/10.1016/j.jas.2003.10.009>.
- Holmden, C., Creaser, R.A., Muehlenbachs, K., 1997. Paleosalinities in ancient brackish water systems determined by ⁸⁷Sr/⁸⁶Sr ratios in carbonate fossils: a case study from the western Canada sedimentary basin. *Geochim. Cosmochim. Acta* 61, 2105–2118. [https://doi.org/10.1016/S0016-7037\(97\)00073-2](https://doi.org/10.1016/S0016-7037(97)00073-2).
- Holmden, C., Hudson, J.D., 2003. ⁸⁷Sr/⁸⁶Sr and Sr/Ca investigation of Jurassic molluscs from Scotland: implications for paleosalinities and the Sr/Ca ratio of seawater. *GSA Bull.* 115, 1249–1264. <http://dx.doi.org/10.1130/B25204.1>.
- Jones, B., 1989. Calcite rafts, peloids, and micrite in cave deposits from Cayman Brac, British-West-Indies. *Can. J. Earth Sci.* 26, 654–664.
- Kambesis, P.N., Coke, J.G., 2013. Overview of the Controls on Eogenetic Cave and Karst Development in Quintana Roo, Mexico, 5, pp. 347–373. https://doi.org/10.1007/978-94-007-5016-6_16.
- Kottek, M., Grieser, J., Beck, C., Rudolf, B., Rubel, F., 2006. World map of the Köppen-Geiger climate classification updated. *Meteorol. Z.* 15, 259–263. <https://doi.org/10.1127/0941-2948/2006/0130>.
- Kovacs, S.E., Reinhardt, E.G., Stastna, M., Coutino, A., Werner, C., Collins, S.V., Devos, F., Le Maillot, C., 2017a. Hurricane Ingrid and tropical storm Hanna's effects on the salinity of the coastal aquifer, Quintana Roo, Mexico. *J. Hydrol.* 551, 703–714. <https://doi.org/10.1016/j.jhydrol.2017.02.024>.
- Kovacs, S.E., Reinhardt, E.G., Werner, C., Kim, S.-T., Devos, F., Le Maillot, C., 2017b. Seasonal trends in calcite raft formation from cenotes Rainbow, Feno and Monkey Dust, Quintana Roo, Mexico: implications for palaeoenvironmental studies. *Palaeogeogr. Palaeoclimatol. Palaeoecol.* accepted.
- Lazar, B., Sivan, O., Yecheili, Y., Levy, E.J., Antler, G., Gavrieli, I., Stein, M., 2014. Long-term freshening of the Dead Sea brine revealed by porewater Cl⁻ and δ¹⁸O in

- ICDP Dead Sea deep-drill. *Earth Planet. Sci. Lett.* 400, 94–101.
- Levinson, A.A., 1968. *Oceans* (Foundations of Earth Science Series). Elsevier Science. [https://doi.org/10.1016/0016-7037\(68\)90037-9](https://doi.org/10.1016/0016-7037(68)90037-9).
- Levy, E.J., Stein, M., Lazar, B., Gavrieli, I., Yechieli, Y., Sivan, O., 2017. Pore fluids in Dead Sea sediment core reveal linear response of lake chemistry to global climate changes. *Geology* 45 (4), 315–318.
- Lighty, R.G., Macintyre, I.G., Stuckenrath, R., 1982. Reef framework: a reliable indicator of sea level in the western Atlantic for the past 10,000 years. *Coral Reefs* 1, 125–130. <https://doi.org/10.1007/BF00301694>.
- McArthur, J.M., Howarth, R.J., Bailey, T.R., 2001. Strontium isotope stratigraphy: LOWESS Version 3: best fit to the marine Sr-isotope curve for 0–509 Ma and accompanying look-up table for deriving numerical age. *J. Geol.* 109, 155–170.
- McDermott, F., 2004. Palaeo-climate reconstruction from stable isotope variations in speleothems: a review. *Quat. Sci. Rev.* 23, 901–918. <https://doi.org/10.1016/j.quascirev.2003.06.021>.
- Medina-Elizalde, M., 2013. A global compilation of coral sea-level benchmarks: implications and new challenges. *Earth Planet. Sci. Lett.* 362, 310–318. <https://doi.org/10.1016/j.epsl.2012.12.001>.
- Medina-Elizalde, M., Burns, S.J., Lea, D.W., Asmerom, Y., von Gunten, L., Polyak, V., Vuille, M., Karmalkar, A., 2010. High resolution stalagmite climate record from the Yucatan Peninsula spanning the Maya terminal classic period. *Earth Planet. Sci. Lett.* 298, 255–262. <https://doi.org/10.1016/j.epsl.2010.08.016>.
- Metcalfe, S.E., O'Hara, S.L., Caballero, M., Davies, S.J., 2000. Records of Late Pleistocene–Holocene climatic change in Mexico - a review. *Quat. Sci. Rev.* 19, 699–721. [https://doi.org/10.1016/S0277-3791\(99\)00022-0](https://doi.org/10.1016/S0277-3791(99)00022-0).
- Milne, G.A., Mitrovica, J.X., 2008. Searching for eustasy in deglacial sea-level histories. *Quat. Sci. Rev.* 27, 2292–2302. <https://doi.org/10.1016/j.quascirev.2008.08.018>.
- Milne, G.A., Peros, M., 2013. Data-model comparison of Holocene sea-level change in the circum-Caribbean region. *Glob. Planet. Change* 107, 119–131. <https://doi.org/10.1016/j.gloplacha.2013.04.014>.
- Moseley, G.E., Richards, D.A., Smart, P.L., Standish, C.D., Hoffmann, D.L., ten Hove, H., Vinn, O., 2015. Early–middle Holocene relative sea-level oscillation events recorded in a submerged speleothem from the Yucatán Peninsula, Mexico. *The Holocene* 1–11. <https://doi.org/10.1177/0959683615585832>.
- Neuman, B.R., Rahbek, M.L., 2007. Modeling the groundwater catchment of the Sian Ka'an reserve, Quintana Roo. *Assoc. Mex. Cave Stud. Bull.* 1, 1–209.
- Palmer, M.R., Edmond, J.M., 1992. Controls over the strontium isotope composition of river water. *Geochim. Cosmochim. Acta* 56, 2099–2111.
- Peltier, W.R., Fairbanks, R.G., 2006. Global glacial ice volume and Last Glacial Maximum duration from an extended Barbados sea level record. *Quat. Sci. Rev.* 25, 3322–3337. <https://doi.org/10.1016/j.quascirev.2006.04.010>.
- Peros, M.C., Reinhardt, E.G., Schwarcz, H.P., Davis, A.M., 2007. High-resolution paleosalinity reconstruction from Laguna de la Leche, north coastal Cuba, using Sr, O, and C isotopes. *Palaeogeogr. Palaeoclimatol. Palaeoecol.* 245, 535–550. <https://doi.org/10.1016/j.palaeo.2006.09.006>.
- Peros, M., Collins S, S., G'Meiner, A.A., Reinhardt, E.G., Pupo, F.M., 2017. Multistage 8.2 kyr event revealed through high-resolution XRF core scanning of Cuban sinkhole sediments. *Geophys. Res. Lett.* 44 <https://doi.org/10.1002/2017GL074369>.
- Perry, E., Paytan, A., Pedersen, B., Velazquez-Oliman, G., 2009. Groundwater geochemistry of the Yucatan Peninsula, Mexico: constraints on stratigraphy and hydrogeology. *J. Hydrol.* 367, 27–40. <https://doi.org/10.1016/j.jhydrol.2008.12.026>.
- Perry, E., Velazquez-Oliman, G., Socki, R., 2003. Hydrogeology of the Yucatán Peninsula. In: *The Lowland Maya Area: Three Millennia at the Human-Wildland Interface*, pp. 115–138.
- Pin, C., Bassin, C., 1992. Evaluation of a strontium-specific extraction chromatographic method for isotopic analysis in geological materials. *Anal. Chim. Acta* 269, 249–255. [https://doi.org/10.1016/0003-2670\(92\)85409-Y](https://doi.org/10.1016/0003-2670(92)85409-Y).
- Pohlman, J.W., Iliffe, T.M., Cifuentes, L.A., 1997. A stable isotope study of organic cycling and the ecology of an anchialine cave ecosystem. *Mar. Ecol. Prog. Ser.* 155, 17–27. <https://doi.org/10.3354/meps155017>.
- Quintana Roo Speleological Survey, 2017. List of Long Underwater Caves in Quintana Roo. Tulum, Quintana Roo Speleological Survey, Mexico. <https://caves.org/project/qrrs/qrlong.htm>.
- Reeve, A.S., Perry, E.C., 1994. Carbonate geochemistry and the concentrations of aqueous Mg²⁺, Sr²⁺ and Ca²⁺: western north coast of the Yucatan, Mexico. *Chem. Geol.* 112, 105–117. [https://doi.org/10.1016/0009-2541\(94\)90107-4](https://doi.org/10.1016/0009-2541(94)90107-4).
- Reimer, P.J., Bard, E., Bayliss, A., Beck, J.W., Blackwell, P.G., Bronk Ramsey, C., Buck, C.E., Cheng, H., Edwards, R.L., Friedrich, M., Grootes, P.M., Guilderson, T.P., Hafflidason, H., Hajdas, I., Hatté, C., Heaton, T.J., Hoffmann, D.L., Hogg, A.G., Hughen, K.A., Kaiser, K.F., Kromer, B., Manning, S.W., Niu, M., Reimer, R.W., Richards, D.A., Scott, E.M., Southon, J.R., Staff, R.A., Turney, C.S.M., van der Plicht, J., 2013. IntCal13 and Marine13 radiocarbon age calibration curves 0–50,000 Years cal BP. *Radiocarbon* 55, 1869–1887. https://doi.org/10.2458/azu_js_rc.55.16947.
- Reinhardt, E.G., Fitton, R.J., Schwarcz, H.P., 2003. Isotopic (Sr, O, C) Indicators of salinity and taphonomy in marginal marine systems. *J. Foraminifer. Res.* 33, 262–272. <https://doi.org/10.2113/33.3.262>.
- Reinhardt, E.G., Stanley, D.J., Patterson, R.T., 1998. Strontium isotopic-paleontological method as a high-resolution paleosalinity tool for lagoonal environments. *Geology* 26, 1003–1006. [https://doi.org/10.1130/0091-7613\(1998\)026<1003:SIPMAA>2.3.CO;2](https://doi.org/10.1130/0091-7613(1998)026<1003:SIPMAA>2.3.CO;2).
- Reinhardt, E.G., Stanley, D.J., Schwarcz, H.P., 2001. Human-induced desalinization of Manzala Lagoon, Nile Delta, Egypt: evidence from isotopic analysis of benthic invertebrates. *J. Coast. Res.* 17, 431–442.
- Smart, P.L., Beddows, P.A., Coke, J., Doerr, S., Whitaker, F.F., 2006. Cave development on the Caribbean coast of the Yucatan Peninsula, Quintana Roo, Mexico. *Geol. Soc. Am.* 2404, 105–128. [https://doi.org/10.1130/2006.2404\(10\)](https://doi.org/10.1130/2006.2404(10)).
- Taylor, M.P., Drysdale, R.N., Carthew, K.D., 2004. The formation and environmental significance of calcite rafts in tropical tufa-depositing rivers of northern Australia. *Sedimentology* 51, 1089–1101. <https://doi.org/10.1111/j.1365-3091.2004.00661.x>.
- Taylor, P., Chafetz, H.S., 2004. Floating rafts of calcite crystals in cave pools, central Texas, USA: crystal habit vs. saturation state. *J. Sediment. Res.* 74, 328–341. <https://doi.org/10.1306/111603740328>.
- Toscano, M.A., Macintyre, I.G., 2003. Corrected western Atlantic sea-level curve for the last 11,000 years based on calibrated ¹⁴C dates from *Acropora palmata* framework and intertidal mangrove peat. *Coral Reefs* 22, 257–270. <https://doi.org/10.1007/s00338-003-0315-4>.
- Toscano, M.A., Macintyre, I.G., 2006. Reply to Gischler E, Comment on Toscano and Macintyre (2005): corrected western Atlantic sea-level curve for the last 11,000 years based on calibrated ¹⁴C dates from *Acropora palmata* framework and intertidal mangrove peat. *Coral Reefs* 22: 257–270(2003), and their response in *Coral Reefs* 24:187–190 (2005). *Coral Reefs* 25, 281–286. <https://doi.org/10.1007/s00338-006-0102-0>.
- van Hengstum, P.J., Reinhardt, E.G., Beddows, P.A., Gabriel, J.J., 2010. Linkages between Holocene paleoclimate and paleohydrogeology preserved in a Yucatan underwater cave. *Quat. Sci. Rev.* 29, 2788–2798. <https://doi.org/10.1016/j.quascirev.2010.06.034>.
- van Hengstum, P.J., Reinhardt, E.G., Beddows, P.A., Schwarcz, H.P., Gabriel, J.J., 2009. Foraminifera and testate amoebae (thecamoebians) in an anchialine cave: surface distributions from Aktun Ha (Carwash) cave system, Mexico. *Limnol. Oceanogr.* 54, 391–396. <https://doi.org/10.4319/lo.2009.54.1.0391>.
- van Hengstum, P.J., Scott, D.B., Gröcke, D.R., Charette, M.A., Bay, G., 2011. Sea level controls sedimentation and environments in coastal caves and sinkholes. *Mar. Geol.* 286, 35–50. <https://doi.org/10.1016/j.margeo.2011.05.004>.
- Ward, W.C., Weidie, A.E., Back, W., 1985. *Geology and hydrogeology of the Yucatan and Quaternary geology of northeastern Yucatan Peninsula*. New Orleans *Geol.Soc* 1–160.